Space Weather®

Peter Thorn has now left the Met Office.

Key Points:

- The satellite risk prediction and radiation forecast (SaRIF) system forecasts the outer electron radiation up to 24 hr ahead, updated every hour
- Risk indicators are provided for four satellite orbits and can be compared against design standards
- The SaRIF system provides a searchable archive of data for anomaly resolution by satellite operators, designers and underwriters

Correspondence to:

R. B. Horne,
rh@bas.ac.uk

Author Contributions:

Conceptualization: Richard B. Horne
Investigation: Richard B. Horne
Software: Sarah A. Glauert
Supervision: Richard B. Horne
Visualization: Richard B. Horne
Writing – original draft: Richard B. Horne
Writing – review & editing: Richard B. Horne

The Satellite Risk Prediction and Radiation Forecast System (SaRIF)

Richard B. Horne[1] , Sarah A. Glauert[1] , Peter Kirsch[1] , Daniel Heynderickx[2] ,
Suzy Bingham[3], Peter Thorn[3], Babara-Ann Curran[3], David Pitchford[4] , Ewan Haggarty[5],
David Wade[6], and Ralf Keil[7]

[1]British Antarctic Survey, Cambridge, UK, [2]DH Consultancy BVBA, Leuven, Belgium, [3]Meteorological Office, Exeter, UK, [4]SES, Betzdorf, Luxembourg, [5]Airbus Defence and Space, Stevenage, UK, [6]Atrium Space Insurance Consortium, London, UK, [7]Rhea Systems GmbH, European Space Agency, Darmstadt, Germany

Abstract With new satellite constellations being launched into low Earth orbit, the growing use of medium Earth orbit for radio-navigation and timing signals, slot region orbits for telecommunications and the introduction of electric propulsion to reach geostationary orbit, there is a growing need to develop services to protect satellites from space weather. Here we highlight two recent events in relation to satellite operations. We summarize 10 user needs that arose out of meetings with satellite operators, designers, underwriters and space agency staff. We present the satellite risk prediction and radiation forecast (SaRIF) system which is designed to meet most of these needs. The system uses real-time data as input to the BAS radiation belt model (BAS-RBM) to solve the Fokker Planck equation and provides a forecast of the electron flux throughout the outer radiation belt with 1-hr resolution up to 24 hr ahead. The electron flux is used to calculate charging currents, and is combined with GOES near real time proton fluxes to calculate dose rate and total ionizing dose behind set levels of shielding for satellites in Medium Earth orbit, Geostationary orbit and slot region orbits. The results are compared against design standards and presented as risk indicators to forecast the risk of damage. The system works automatically and is updated every hour. We also present data and a best reconstruction of the radiation environment which are held in a searchable archive for satellite anomaly resolution. The SaRIF system is available via the European Space Agency space weather web portal.

Plain Language Summary With new satellite constellations being launched into low Earth orbit, the growing use of other orbits and the introduction of electric propulsion, we need to protect satellites from space weather. Here we highlight two recent events in relation to satellite operations. We summarize 10 user needs that arose out of meetings with satellite operators, designers, underwriters and space agency staff. We present the satellite risk prediction and radiation forecast (SaRIF) system which is designed to meet most of these needs. The system uses real-time data as input to the BAS radiation belt model (BAS-RBM) and provides a forecast of the electron flux throughout the outer radiation belt with 1-hr resolution up to 24 hr ahead. The electron flux is used to calculate charging currents, and is combined with GOES near real time proton fluxes to calculate dose rate and total ionizing dose behind set levels of shielding for satellites on orbit. The results are compared against design standards and presented as risk indicators to forecast the risk of damage. The system works automatically and is updated every hour. We also present a best reconstruction of the radiation environment which are held in a searchable archive for satellite anomaly resolution.

1. Introduction

On 7 April 2019 Intelsat 29e, a communications satellite at geostationary orbit, experienced an anomaly resulting in a fuel leak. Two days later communication with the satellite was lost, and as revealed by ground based optical telescopes, a number of pieces of debris were seen emanating from the satellite in the days that followed (https://www.spaceflightnow.com/2019/04/15/stricken-with-fuel-leak-intelsat-29e-seen-drifting-in-geostationary-orbit/). ExoAnalytic's observations are available on YouTube (https://www.youtube.com/watch?v=aqPrVn71IqY). On 10 April Intelsat issued a Press Release reporting a service outage which affected maritime, aeronautical and wireless operator customers in the Latin America, Caribbean and North Atlantic regions. They also described their efforts to migrate customers to other satellites (https://www.intelsat.com/news/press-release/intelsat-29e-service-outage/). On 18 April Intelsat declared the satellite a total loss. The satellite now appears to be tumbling out of control and drifting toward the East around the geostationary arc.

The complete loss of a satellite in geostationary orbit (GEO) is exceptional, but not unique. There are a number of other examples (e.g., see Horne, Glauert, et al. [2013]). But in this case the uncontrolled drift of what remains of Intelsat 29e together with debris from the event is a particular concern as they pose a risk of collision with other satellites. Geostationary orbit is one of the most highly populated orbits with over 560 operational satellites as of 1 August 2020 (Union of Concerned Scientists Satellite Database, http://ussusa.org/resources/satellite-database) and there is no prospect of obit decay or reentry by natural means. Orbital predictions, collision warning and avoidance maneuvers by other satellites will now become essential.

What is interesting about this event is that there were two anomalies within a few days; one related to the fuel leak and the other associated with the production of debris. Following the failure review, Intelsat and Boeing (the satellite manufacturer) proposed two potential reasons for the loss of Intelsat 29e, one of which was the impact of a micrometeoroid, the second of which was an electrostatic discharge coupled with a flaw in a wiring harness (https://spacenews.com/intelsat-pins-intelsat-29e-failure-on-external-event-readies-replacement-order/). Intelsat recorded a US$ 382 million asset impairment charge for the loss of Intelsat 29e and reported a loss of annual revenue of US$ 45 to 50 million. Since the spacecraft was only three years into its operational life, and satellites at GEO usually operate for 15 years or more, it is very important to establish the cause of the anomaly in order to prevent anything like this happening again.

One of the most important requirements for the investigation team is access to the data necessary to identify the cause of the anomalies. Satellite telemetry can provide a wealth of information to guide the investigation but to rule out space weather also requires information on the space environment. This information is not always easy to access as it may be held in different forms in different locations. Even when it is available it requires careful interpretation and expertize to rule out space weather.

While recent history of the space environment is one of the requirements for the investigation team, space weather forecasts are also required by satellite operators in order to take preventative action. A recent example involves SKYNET 4E. On 7 September 2017 SKYNET 4E was scheduled to commence a series of maneuvers, initiating transit from its current operating slot in geosynchronous orbit so that an incoming satellite could take up that position. Just before Midnight on 4 September 2017, Operators received a forecast from the UK Met Office (UKMO) of a large CME that was due to arrive at Earth on or around 6 September 2017. The Forecasters could not provide a prediction of the polarity of the interplanetary magnetic field or how effective the CME would be, but they did know from previous experience that a large CME can cause a large magnetic storm that enhances the electron flux in the radiation belts persistently for a day or more (e.g., Reeves et al. [2003]). From long-term tracking of the performance of electronic components on SKYNET 4E by the Operators, they knew that units required for the maneuvers had a sensitivity to anomalous behavior during high electron flux: moving the spacecraft as the CME reached the Earth with these units switched on was a risk and there was no option to delay the arrival of the incoming satellite.

The Operators had two choices: do nothing and accept the risk that the CME was geoeffective, or elect to move SKYNET 4E before the electron flux had a chance to increase. It was not certain that the SKYNET 4E would be affected, but if it did suffer an anomaly during maneuver there was a possibility it could require recovery action taking several days. The impact could be that its position would be uncontrolled, leaving it in unplanned proximity to the incoming satellite and possibly other neighboring ones.

The Operators promptly decided to control the risk and within the very tight timeframe the UKMO forecast had provided, replanned and executed the SKYNET 4E maneuver so it concluded before the forecast CME arrival. As it turned out there was a strong magnetic storm which started on 7th and lasted until 11th, but no major increase in electron flux. The principle here is that the Operators took the course of action that minimized risk, informed by both the best forecasting advice provided by the UKMO and their own developed understanding of the potential environmental impact on their SKYNET 4E satellite.

The example above illustrates the importance of space weather forecasts. It also illustrates the difficulty of quantifying the value of space weather forecasts (see also Oughton et al. [2019]). No anomalies were recorded and no financial loss or reputational damage was incurred. But, as the Operators pointed out, controlling the risk effectively removed the potential anomaly and allowed a course of action with increased operational assurance.

These two events illustrate the importance of forecasting space weather for satellite operations and providing data to help identify the cause of a satellite anomaly. The purpose of this paper is to introduce a new system called SaRIF which is designed to improve forecasting capability and provide a searchable archive of data and model results to help anomaly resolution. SaRIF is an acronym for satellite risk prediction and radiation forecast system and is available via the European Space Agency (ESA) web portal (currently compatible with Safari 15.1 and Firefox 93.0) after obtaining an ESA login account (https://swe.ssa.esa.int/web/guest/sarif-federated) for. In the following sections, we describe some of the existing services and provide a report on user requirements that were identified from a series of consultations with satellite operators, designers, underwriters and space agency staff. We describe the overall SaRIF system and how it works and provide examples of some of the results that users can access online. The system is built around the BAS radiation belt model which provides a forecast of the radiation belt flux and which is described in more detail in a companion paper (Glauert et al., 2021). The model is supplemented with near real time proton flux from the GOES satellites obtained from the NOAA Space Weather Prediction Center (SWPC). In the discussion, we suggest a number of areas where more research into the basic physics and application of machine learning and artificial intelligence methods will help improve the forecasts and the reconstructions. We assess the extent to which SaRIF fulfills user needs and suggest where the system should be developed further to help protect satellites on orbit.

2. Background

The relativistic electron forecast model (REFM) is perhaps one of the best known forecasting systems for satellites. These forecasts are available from the NOAA/SWPC (https://www.swpc.noaa.gov) and the Space Weather Prediction Center at the UKMO (https://www.metoffice.gov.uk/public/weather/space-weather/). It is also now available via the SaRIF system, as described below. The REFM provides a forecast of the 24 hr electron fluence greater than 2 MeV at geosynchronous orbit for up to 3 days ahead. It also provides a comparison between the forecast and what was actually measured by one of the GOES satellites. The model is based on a linear prediction filter method (Baker et al., 1990) and has been evaluated against several measures of forecasting skill, as given on the web site.

Although the REFM model provides an excellent service for GEO there are a number of reasons why we need to develop an improved forecasting system for GEO, and for other orbits. For example, there are satellite constellations in inclined medium Earth orbit (MEO) providing signals for positioning, navigation and timing. These include the well-known GPS system as well as the European Galileo, Russian GLONASS, and Chinese BeiDou systems. There are satellites in circular equatorial orbit in the slot region at altitudes of 6,000–8,000 km such as the O3b constellation, and in highly elliptic Earth orbit (HEO) used for broadcasting, and internet. There are also several hundred satellites in low Earth orbit (LEO) used for Earth observation and other applications, including the new communication constellations being launched. These include the Starlink constellation at 550 km (https://en.wikipedia.org/wiki/Starlink) and the OneWeb constellation at 1,200 km (https://www.oneweb.world/technology) which are being developed to provide global internet services. These orbits need the development of new and better forecasting capability.

Another important reason for new forecasting services is the growing use of satellites with electric propulsion. Although electric propulsion has been used for scientific and technology demonstration satellites for many years, such as SMART-1 which went to the moon, commercial satellites with all-electric propulsion were first introduced in 2015. In this case, the satellites take 200 days or more to reach GEO and can experience significant radiation exposure leading to loss of solar array power before reaching final orbit (Horne & Pitchford, 2015; Lozinski et al., 2019). Since the radiation environment for MEO, LEO or HEO is orders of magnitude different to that in GEO there is a need to develop new services.

One of the first systems to provide information for other orbits was the EU SPACECAST project (Horne, Glauert, et al., 2013). This system provided a 3-hr forecast of the MeV electron flux throughout the outer radiation belt from 2 to 7 Re relevant to internal satellite charging. It also provided a nowcast of the low energy electron flux for surface charging and an archive of data that could be viewed retrospectively. The system started operating in 2013. This system used physical models such as the BAS radiation belt model (BAS-RBM) to forecast high energy relativistic electrons (Glauert et al., 2014b) and IMPTAM to provide a nowcast of lower energy electrons (Ganushkina et al., 2015). These models included the effects of wave-particle interactions which were shown to

improve the accuracy of the forecasts (Horne, Glauert, et al., 2013). The SPACECAST project came to an end in 2014 but the forecasting element continued in a subsequent EU project called SPACESTORM. The primary purpose of SPACESTORM was to investigate the effects of extreme space weather events in relation to satellites (e.g., Hands et al., 2018; Horne et al., 2018). However, the new innovation in SPACESTORM was to bring together the radiation environment with radiation effects on materials used in satellites. SPACESTORM introduced the idea of risk indicators which are tailored to the needs of satellite operators and designers. SPACESTORM came to an end in 2017.

There have been other projects that have developed on-line forecasting. For example, the EU PROGRESS project used an artificial intelligence method known as NARMAX to forecast the 24 hr electron fluence at GEO and claims to have a higher skill score for GEO than the REFM model (Balikhin et al., 2016; Boynton et al., 2016). They also use the VERB model to calculate the electron flux for the outer radiation belt (Subbotin & Shprits, 2009).

The success of the SPACESTORM project in bringing together the radiation environment with radiation effects on materials attracted the attention of the European Space Agency (ESA). The ESA subsequently funded the development of a pre-operational system called SaRIF, which incorporated the forecasting element with a more extensive and easily searchable online archive of data.

3. User Requirements

To ensure that the SaRIF system met user needs two user meetings were organized to gather information. The first took place at the European Space Operations Center (ESOC) in Darmstadt, Germany on 14 June 2017, and the second at the offices of Inmarsat in London on 30 June 2017. Representatives from several organizations including satellite operators from ESOC, SES, EUMETSAT and Inmarsat attended the meetings. The results, together with an earlier discussion with underwriters at Lloyds of London on 5 January 2016, and a series of discussion sessions at the European Space Weather Week, were used to compile a set of user requirements which can be summarized as follows:

1. Space weather is one of many different factors that satellite operators must consider. As a result, operators wanted a high-level color-coded display that would indicate the risk of damage due to space weather. If the displays were green, then they could continue with their work.
2. If a significant risk were indicated on the high-level display then users wanted the ability to drill down for more information to understand and evaluate the risk.
3. Users wanted a system that was more tailored to their needs than current forecasting systems. A set of risk indicators were identified which include surface charging, internal charging, total ionizing dose, single event upsets and solar array degradation. Provision of these risk indicators was considered a step change improvement over previous measures such as electron fluence since they combine the radiation environment with radiation effects on satellites and hence target particular risks.
4. Users wanted risk indicators that are quantifiable and presented in a simple display. Furthermore, the risk should be compared against a design standard or some other form of reference.
5. The system should provide risk indicators for different types of orbits including GEO, MEO, slot region, HEO, and LEO. For internal charging and radiation dose GEO, MEO and slot region orbits were considered the most important.
6. Users wanted risk indicators calculated along the orbits of particular satellites where possible so that they could be compared against their own propriety information and knowledge regarding the susceptibility of their satellites to environmental threats.
7. Users wanted an interactive interface with the ability to drill down and examine the electron and proton energy spectra incident on the spacecraft. This would help identify charging events due to unusually high particle energies and help determine whether the radiation environment was the likely cause of a satellite anomaly.
8. Users wanted forecasts for up to 24 hr ahead and longer if possible. This would give operators time to take mitigating action, for example, to plan their operations and have additional staff available to deal with any problems, re-schedule maneuvers or software updates. Even if a reliable forecast could not be achieved on this timescale current situation awareness was considered extremely important. Situation awareness would help prevent operators from taking action during a space weather event that would make the situation worse.

9. Users wanted a searchable archive of data that could be interrogated after an event. This was to help determine the cause of an anomaly, and to look for associations between anomalies and the space environment.
10. Users wanted the ability to download data and do their own analysis. This would enable operators, designers and underwriters to investigate periods when an anomaly had taken place without revealing the satellite, time or place, or other information considered sensitive.

4. Forecasting Model

To meet most of the user needs a system was designed that could forecast the high energy electron radiation belts in real time, combine with radiation effects on materials and provide an archive of data for post event analysis. The effects of proton radiation were also included. At the heart of this system is the British Antarctic Survey Radiation Belt Model (BAS-RBM) (Glauert et al., 2014b). The code was specially adapted from a research model into a forecasting model that can forecast up to 1 day ahead.

The BAS-RBM is similar to previous models that have been developed to study the Earth's radiation belts such as Salammbô (Beutier & Boscher, 1995), VERB (Shprits et al., 2009) and DREAM (Reeves et al., 2012; Tu et al., 2013, 2014, 2019). The model solves the Fokker Planck equation to calculate the time evolution of the electron phase space density which is then converted into an electron flux and compared against observations. The code is based on the conservation of the three adiabatic invariants and therefore uses a magnetic coordinate system rather than a geographic coordinate system. Non-dipole magnetic field effects are captured by transforming satellite data into a magnetic coordinate system using a magnetic field model (Olson & Pfitzer, 1977) and then analyzing that data to generate the initial conditions, the boundary conditions and the diffusion coefficients. Once this transformation is done the model uses a dipole magnetic field internally to calculate the electron flux, as is common for all these types of global radiation belt models. The primary output from the model is the electron differential flux as a function of energy over a range of magnetic coordinates from $L^* = 2$ to $L^* = 7$, where L^* is Roederer's L^* (Roederer, 1967), corresponding very approximately to 2–7 Re during geomagnetically quiet conditions. Thus the outer boundary lies outside geostationary orbit (6.6 Re). The model output covers an energy range that varies with distance from the Earth due to the geomagnetic coordinate system but has a minimum energy of 150 keV at the outer boundary. The high energy boundary is set at 30 MeV everywhere. The output covers pitch angles between 0° and 90° and assumes symmetry about 90° for the northern and southern hemisphere. More details of the model and the coordinate system can be found in a companion paper (Glauert et al., 2021).

The BAS-RBM includes several physical processes. They include radial diffusion driven by ULF waves which govern transport across the geomagnetic field, resonant wave-particle interactions which cause pitch angle and energy diffusion and are responsible for electron acceleration and loss, Coulomb collisions with the atmosphere which also cause pitch angle diffusion and loss, and losses due to electrons that cannot complete a closed drift path all the way round the Earth. The latter usually occurs due to inward motion of the magnetopause boundary which we will refer to here as magnetopause losses.

Four different types of plasma waves are included in BAS-RBM as sub-models. They are the pitch angle and energy diffusion rates calculated using the PADIE code (Glauert & Horne, 2005) from a statistical analysis of plasma waves measured by satellites over several years. They are a chorus wave model (Horne, Kersten, et al., 2013), a plasmaspheric hiss model (Glauert et al., 2014b), a lightning generated whistler (LGW) model (Glauert et al., 2014b), and an electromagnetic ion cyclotron wave (EMIC) model (Kersten et al., 2014). The wave models include wave properties that vary with L^*, magnetic local time, latitude and geomagnetic activity and are applied to a drift averaged electron distribution function. BAS-RBM does not include transport due to convection electric fields and thus it is only valid for energies greater than about 150 keV, although there could be an important contribution due to convection during very disturbed geomagnetic conditions (Allison et al., 2017). The model uses the electromagnetic radial diffusion coefficients from Brautigam and Albert (2000) and a magnetopause model from Shue et al. (1998) with the adaptions described by Glauert et al. (2014a).

The diffusion coefficients used in BAS-RBM depend on the Kp index as does the electron flux at the inner boundary at $L^* = 2$. Kp was chosen since the UKMO provide a forecast of Kp and hence the model can be used to forecast the radiation belts by using this data-stream. The flux is set to zero on the high energy boundary. The flux on the outer boundary is determined from the > 800 keV electron flux measured in real-time by GOES 15. The

measured flux is used to select a differential flux spectrum that was developed from a statistical analysis of fitting Lorentzian "kappa" distributions to the GOES 15 data set similar to the method described in Glauert et al. (2018). The measured > 800 keV flux is used to interpolate between the two nearest spectra. This has now been updated using the differential electron flux from GOES 16 which will be released later in 2021. An algorithm is used to approximate the location of the last closed drift shell based on the dynamic solar wind pressure and IMF Bz. If the last closed drift shell moves inside $L* = 7$, for example, due to inward motion of the magnetopause, then an additional loss term is applied to account for the loss of electrons on open drift shells. Full details of the model are given by Glauert et al. (2014a). The flux as a function of $L*$ on low energy boundary is an average profile and is scaled so as to match the flux at the outer boundary.

It is important to understand that the code is only valid for conditions where diffusion is valid or is a reasonable approximation. Perhaps one of the most important restrictions is that the timescale must be longer than several drift periods. Since the timescale for variations in the radiation belts is usually several hours which is much longer than the timescale for a 1 MeV electron to drift around the Earth at geostationary orbit (approximately 10 min) the system is valid most of the time. However, there are unusual events where the code is not valid. For example, in March 1991 a new radiation belt was formed within 2 min due to a rapid compression of the geomagnetic field (Blake et al., 1992). In this event the electrons were accelerated by an induced electric field caused by the rapid compression of the geomagnetic field and "surfed-in" toward the Earth during a fraction of their drift orbit (Hudson et al., 1995). This physical process is not included in the code. However, after such a rapid compression the code can be used to examine the decay of the belts which usually takes place on a much longer timescale.

5. System as a Whole

Figure 1 shows the SaRIF system schematically. Several data-streams are collected in near real-time to drive the BAS-RBM. These include a forecast of Kp from the UKMO for up to one day ahead, a near real-time Kp, the solar wind speed, density and IMF Bz (shown in light yellow). Several other real-time data-streams are also collected to help interpretation of the radiation environment and validate the forecast, as described later. Real-time data is accessed every hour and held in a data repository (dark blue). The forecast of Kp is used to select the diffusion coefficients used in the BAS-RBM which have been pre-computed, and to update the inner boundary conditions for the next 24 hr. In general the electron flux spectrum on the outer boundary is assumed to persist for 24 hr, but with additional algorithms to account for magnetopause compressions. More details can be found in the companion paper (Glauert et al., 2021).

After downloading and pre-processing the data a number of quality checks are conducted, for example, to check for missing data. If data are missing then the last good data are used. The data are then used to run the BAS-RBM (purple) on the computer system in the UK (JASMIN, https://www.jasmin.ac.uk) and the output stored in the data repository. Each run is for the last 7 days plus a forecast of 1 day with a time resolution of 10 min. The forecast of Kp provided by the UKMO is used for the forecast period and near real-time Kp provided by the Helmholtz Center, Potsdam is used for the last 7 days. The model output is then provided to the Environment Model Event Coupling (EMEC) suite of software to calculate the radiation effects.

EMEC operates an Open Data Interface (ODI) with a MySQL database. ODI provides a common interface for space environment data sets (https://essr.esa.int/project/odi-open-data-interface-server) that downloads and stores GOES near real time proton fluxes from SWPC. The ODI software suite comprises tools to generate state vectors (i.e., position and velocity) from two line element (TLE) data published by Space Track (https://www.space-track.org/) using NAIF/SPICE (https://naif.jpl.nasa.gov/naif/) and software to calculate $L*$ (UNILIB, https://www.mag-unilib.eu/). Every hour, coordinates for the four reference spacecraft (GOES 14, GOES 15, GIOVE-A, and O3b-12) are calculated at one minute resolution using TLEs. UNILIB is used to calculate $L*$ using the IGRF and Olsen-Pfitzer quiet magnetic field model (Olson & Pfitzer, 1977). Since there can be small differences between $L*$ calculated using UNILIB and IRBEM (even for the same field model) the values from UNILIB are re-scaled in accordance with the $L*$ definition used in IRBEM. This is done to be compatible the wave diffusion matrices which were computed using IRBEM. $L*$ is used to interpolate the BAS-RBM model outputs. The resulting electron flux are used to calculate the charging current behind a given level of Al shielding using the DICTAT code (Rodgers et al., 2000). Dose rates are obtained by running the SHIELDOSE-2Q code (Seltzer, 1980) on the electron spectra and the GOES proton spectra.
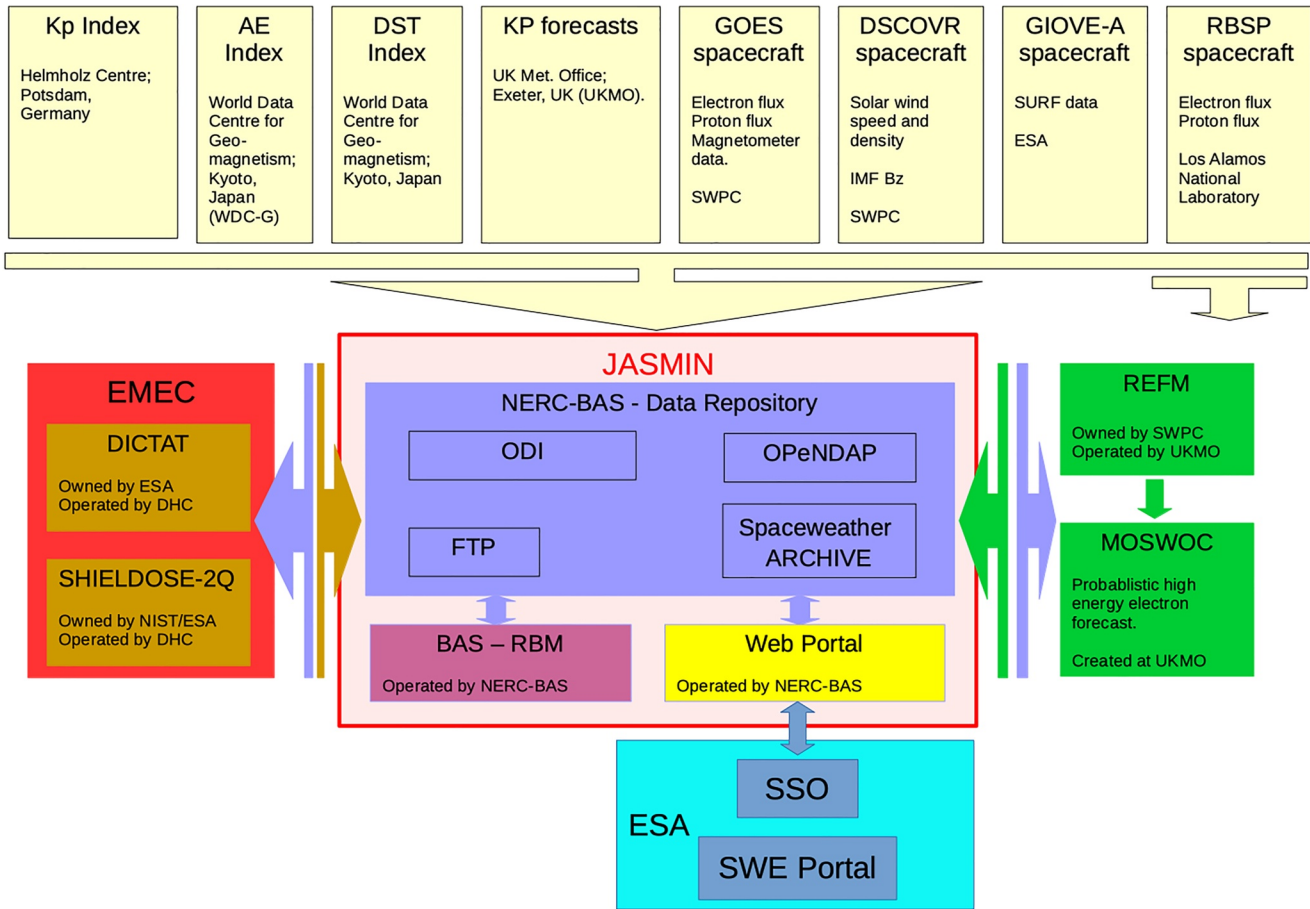
Figure 1. Schematic view of the SaRIF system. Several real-time data-streams are collected from external sources (light yellow) and held in a data repository (dark blue) which includes data retrieval (OPeNDAP) and an Open Data Interface (ODI). Data are passed to run the BAS-RBM (purple) and output returned for access by the EMEC software suite (red) to calculate the radiation effects and risk indicators. The results are archived along with the supporting data (dark blue) and displayed on the federated web site (yellow). The displays can be accessed via the ESA SWE portal by a single sign on (SSO) system and navigating to find SaRIF. Results from the REFM model (green) are also displayed on the web site.

To find the proton spectrum in lower orbits the magnetospheric shielding tool used in SEPEM (http://www.sepem.eu/) is used to calculate the rigidity and the corresponding geomagnetic attenuation factor averaged over the spacecraft orbit and applied to the GOES proton spectrum. As the proton flux is based on measurements, the proton flux for the forecast period is set equal to the measured flux over the last hour. EMEC then feeds back the charging currents and dose rates to the SaRIF server. The results are then compared to design guidelines provided by the European Cooperation for Space Standardization (ECSS, 2020), and the NASA Technical Handbook (NASA, 2011) and assigned a level of risk which may be green, yellow, amber or red. Two risk indicators are presented, one for internal charging and one for dose rate. The data, model and the risk indicators are then displayed along with other supporting information on the web (Figure 1, yellow) which can be accessed via the ESA web portal (turquoise) by navigating to find SaRIF. The SaRIF web display also includes results from REFM run by the UKMO (green).

The total time taken to collect the data, run BAS-RBM, do the data transfers, calculate the risk indicators and update the web displays is less than 15 min. Within this time interval there is a delay between each process to help ensure that each one is completed before starting the next. The cycle is repeated every hour.

As it takes up to 2 weeks for a definitive value of Kp to be produced by the Helmholtz Center, Potsdam, a post event reconstruction of the radiation belts is carried out every week for the period up to two weeks prior to the current time. If Kp from Potsdam is not available then Kp from NOAA/SWPC is used as a backup. The post event reconstruction is held in a searchable archive as a resource to help identify the cause of a satellite anomaly.
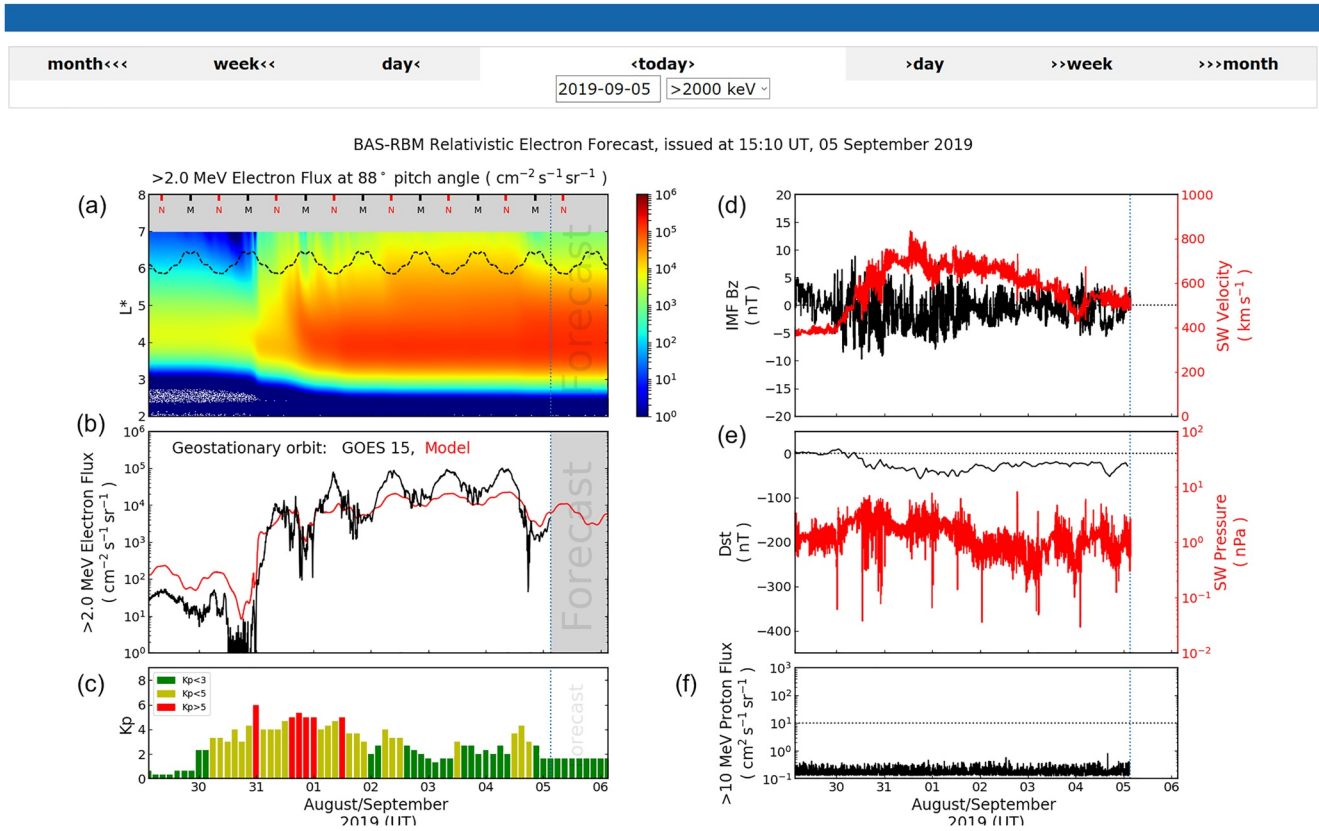
Figure 2. Radiation environment showing (a) the integral electron flux >2 MeV color coded as a function of L^* and time, (b) the integral electron flux >2 MeV measured by GOES 15 (black) and from the model (red), (c) the Kp index, (d) the IMF Bz (black) and solar wind velocity (red), (e) Dst index (black) and solar wind pressure (red), and (f) integral proton flux >10 MeV for GOES 15. The track of GOES 15 is shown by the dotted line in (a) together with an indication of when GOES 15 crosses noon (N) and midnight (M). The forecast period is to the right of the vertical dotted line and illustrated more clearly by the gray area in (b). The model results shown prior to the forecast are the simulation of the flux at GOES 15 using boundary conditions at $L^* = 7$.

The SaRIF system started operating in January 2019. During the testing phase in 2019 the model ran automatically providing forecasts every hour and had to be re-started 6 times over a 9-month period. The down times lasted typically an hour or so and were mostly associated with computer upgrades on local computers not intended for continuous operational service.

At the end of 2019 GOES 14 and 15 were taken out of service and replaced by GOES 16 and 17. This caused a major disruption to SaRIF since GOES 16 and 17 do not provide measurements of the integral electron flux >800 keV which were used to specify the outer boundary of the model. Instead, they provide the differential flux at a number of energies which is much more desirable, but required additional work to include the new data formats and analysis to develop a new procedure to specify the outer boundary. In December 2020, the system was transferred to run using Amazon web services which is more suitable for operational services and has so far proved to be very robust. The new system, adapted to include GOES 16 and 17, will be released later in 2021 and described elsewhere. The rest of this paper describes the system using examples from GOES 14 and 15.

6. Radiation Environment Forecasts

Figure 2 shows an example of one of the forecasts provided for 5 September 2019. Figure 2a shows the electron integral flux >2 MeV for a 7-day period prior to 5 September plus the one-day forecast to the right of the dashed vertical line (it is also possible to select the integral flux >800 keV and the differential flux at 800 keV and 2 MeV). The panel provides a summary of the flux throughout the slot region ($2 < L^* < 3$) and outer electron belt out to $L^* = 7$, calculated using the Olsen-Pfitzer magnetic field model (Olson & Pfitzer, 1977). During 31 August, the model shows there was a significant increase in electron flux throughout the outer belt which

continued until the end of the fourth and was forecast to continue until the end of 5 September. Figure 2b shows a more quantitative comparison between the model (red) and observations (black) made by GOES 15 (Note that the model results shown in Figure 2b prior to the forecast are the simulation of the flux at GOES 15 using boundary conditions at $L^* = 7$ and not that forecast by the model. This was requested by the users. The forecasting skill is discussed separately below). As the flux varies with longitude along geostationary orbit the flux has been calculated for the longitude of GOES 15. Although the model results are initially higher than the flux the model captures the flux drop-out on 30 September and the rapid increase on 31st. There is clearly a much larger diurnal variation in the flux measured by GOES 15 than the model, but the model reproduces the reduction in flux on the 4th September and forecast a lower level with a diurnal variation for the next 24 hr. The diurnal variation is caused by the variation in L^* along the track of the satellite as shown by the dashed line in Figure 2a. To a first approximation in a static magnetic field electrons drift around the Earth along a line of constant magnetic field and are farther away on the dayside due to the stronger field. Thus, on the dayside GOES 15 measures electrons with a lower L^*, as indicated by "N" for noon in Figure 2a. As the electron flux usually peaks near $L^* = 5.5$ (Reeves et al., 2013) the flux is usually much higher at noon on the dayside. The larger diurnal variation measured by GOES is due to a combination of a more distorted magnetic field during this event and a change in the electron spectrum that is not fully captured in the model.

The other panels in Figure 2 provide supporting data to help interpretation. The Kp index (Figure 2c) shows there was a significant increase in geomagnetic activity on 30 September some 12 hr or so before the flux drop-out, and generally increased further on 31st as the flux increased. This coincided with a weak magnetic storm that started on the 30th as shown by the reduction in the Dst index (Figure 2e). However, this was only a weak storm as Dst did not drop much below -50 nT. More importantly there was a significant increase in the solar wind speed above 500 km s^{-1} on 30th (Figure 2d) which peaked near 800 km s^{-1} and remained high until the end of the event. The fast solar wind stream was accompanied by large fluctuations in IMF Bz and a small increase in solar wind pressure (Figure 2e).

A fast solar wind stream is well known to be associated with a significant and prolonged increase in the radiation belts and periods known as high intensity long duration continuous auroral activity or HILDCAA events (Tsuru-tani & Gonzalez, 1987). In fact, they can drive some of the highest increases in the radiation belts fluxes (Horne et al., 2018). In outline, Alfven wave type fluctuations in the solar wind couple energy into the geomagnetic field via intermittent reconnection and is later released in a series of substorms and periods of enhanced convection. Electrons at energies of tens of keV driven by electric fields, and higher energy electrons transported by radial diffusion, form the seed and source populations respectively. These electrons are further accelerated to radiation belt energies by wave-particle interactions (Horne et al., 2005; Meredith et al., 2001).

Figure 2f shows the proton flux >10 MeV also measured by GOES 15. When the integral proton flux exceeds approximately 10 cm^{-2} s^{-1} sr^{-1} the >2 MeV electron flux measured by GOES 15 is contaminated and unreliable. Thus, the proton flux provides a measure of data quality as well as being an indicator of a solar energetic particle (SEP) event. During this event there were no SEP events.

Figure 3 shows the same period but with data from GIOVE-A. GIOVE-A is one of the test Galileo radio naviga-tion satellites in a circular inclined orbit at an altitude of approximately 23,322 km (after 2012) and inclination of 56°. As a result, these satellites pass through the radiation belts twice on each orbit as shown in Figure 3a where the track goes from high to low L^*. The lowest L^* is reached as they cross the magnetic equator which is nominally around $L^* = 4.66$ but is generally lower on the dayside and higher on the nightside due to the dayside compression of the geomagnetic field. GIOVE-A carries a charge plate detector which measures the charging current under three levels of shielding, equivalent to 0.5, 1.0 and 1.5 mm of Al (Ryden et al., 2008). Rather than convert the observations to flux, the charging plate current is shown (Figure 3b) as this can be compared to design standards for internal dielectric charging published by the ESA (ECSS, 2020) and NASA (NASA, 2011). Electron flux from the model is converted to plate current for comparison, as shown below.

Unfortunately, GIOVE-A has reached the end of mission and while data is still being downloaded it is intermit-tent. It is however one of the very few data sets available in near real time in the heart of the radiation belts. Other satellites such as the operational Galileo system have similar detectors but since data are downloaded in the public regulated service datastream they are not available, either in real time or otherwise without signing non-disclo-sure agreements. Particle detectors are also carried on the GPS satellites but again are not available in real time.
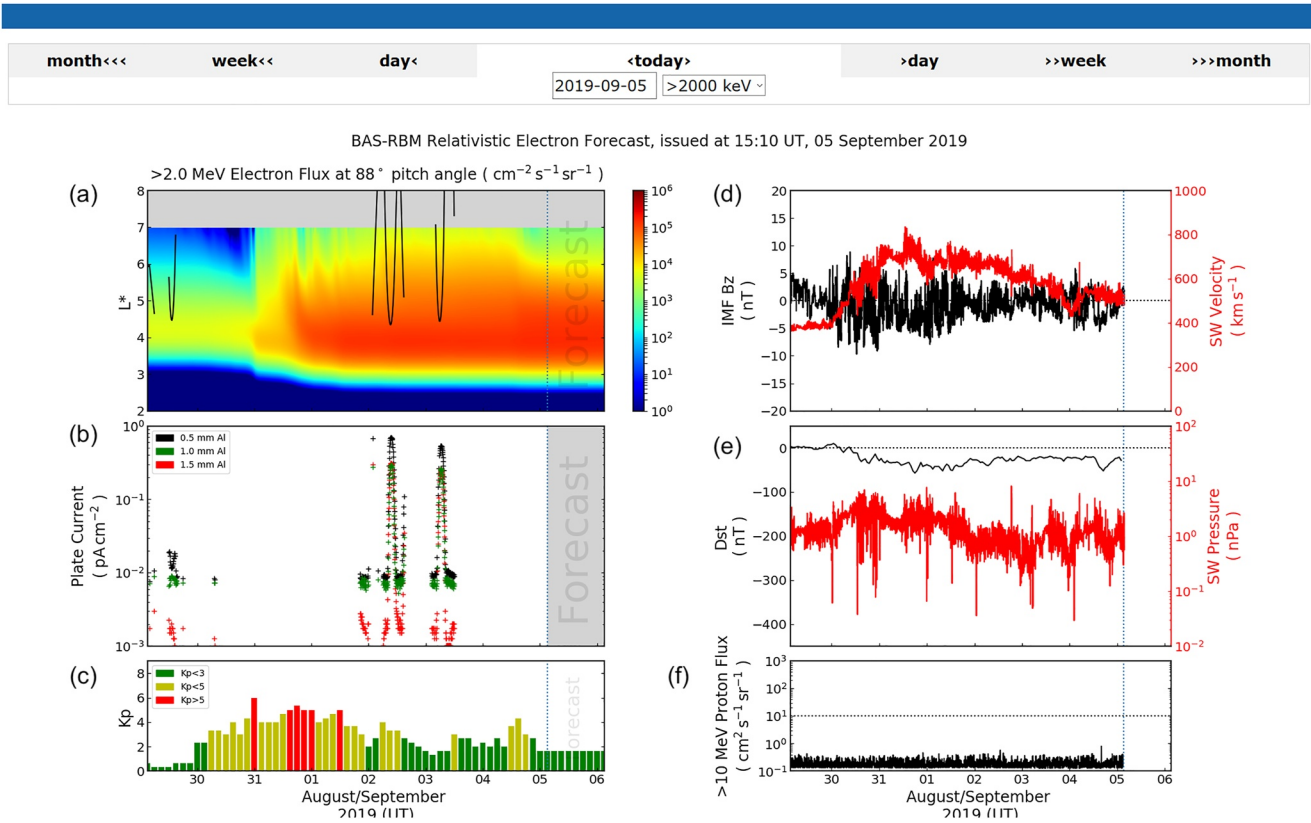
Figure 3. Same as Figure 2 but the track of GIOVE-A is shown in (a) and the measured charging currents in (b) behind 0.5, 1.0 and 1.5 mm of Al shielding.

7. Internal Charging

One of the most important risks to satellites in geostationary orbit and medium Earth orbit is internal charging (also known as deep dielectric charging) caused by high energy electrons. During periods of high electron flux internal charging can lead to an electrostatic discharge and permanent satellite damage (Iucci et al., 2005; Wrenn, 1995). The sensitivity of satellites to internal charging varies according to orbit, choice of components and design and the amount of radiation shielding. The integral electron flux >2 MeV is often used as an indicator of the risk of internal charging, particularly when the flux exceeds a given level (Wrenn, 2009). However, there are several other factors that are also important, such as the electron energy spectrum, the level of shielding and the dielectric materials used in a satellite. In the SaRIF system we have taken a step forward to convert measurements of the environment into something more tailored to user needs by calculating the amount of internal charging behind a specified level of shielding. The advantage of using internal charging currents is that they can be compared to design standards, and thus converted into a risk index.

Typically, the satellite skin, which may be in the form of a honeycomb panel, offers an equivalent of 0.5 mm of Al shielding. Sensitive electronic components are usually placed inside a shielded box and may have an additional 1.5 mm of Al shielding or more depending on the orbit and the electron flux. Therefore, connectors outside the box are likely to pose a greater risk. A shielding of 0.5 mm of Al was therefore selected for calculating internal charging. Figure 4 shows an example of the charging current for GOES 14 for the same period as before. In this case the energy spectrum was constructed from the differential electron flux from BAS-RBM at the location of GOES 14 between 0.15 and 10 MeV, together with measurements of the >800 keV and >2 MeV integral flux measured by GOES 14. The internal charging current deposited in Kapton was calculated using the DICTAT radiation effects code assuming planar geometry.

Figure 4 shows that the charging current exceeded 0.1 pA cm^{-2} just before 1 September 2019 and except for a short excursion on the first remained above that level until late on 5 September. The European standard (ECSS, 2020) recommends shielding for some components if the charging current exceeds 0.02 pA cm^{-2} and 0.1 pA cm^{-2} for
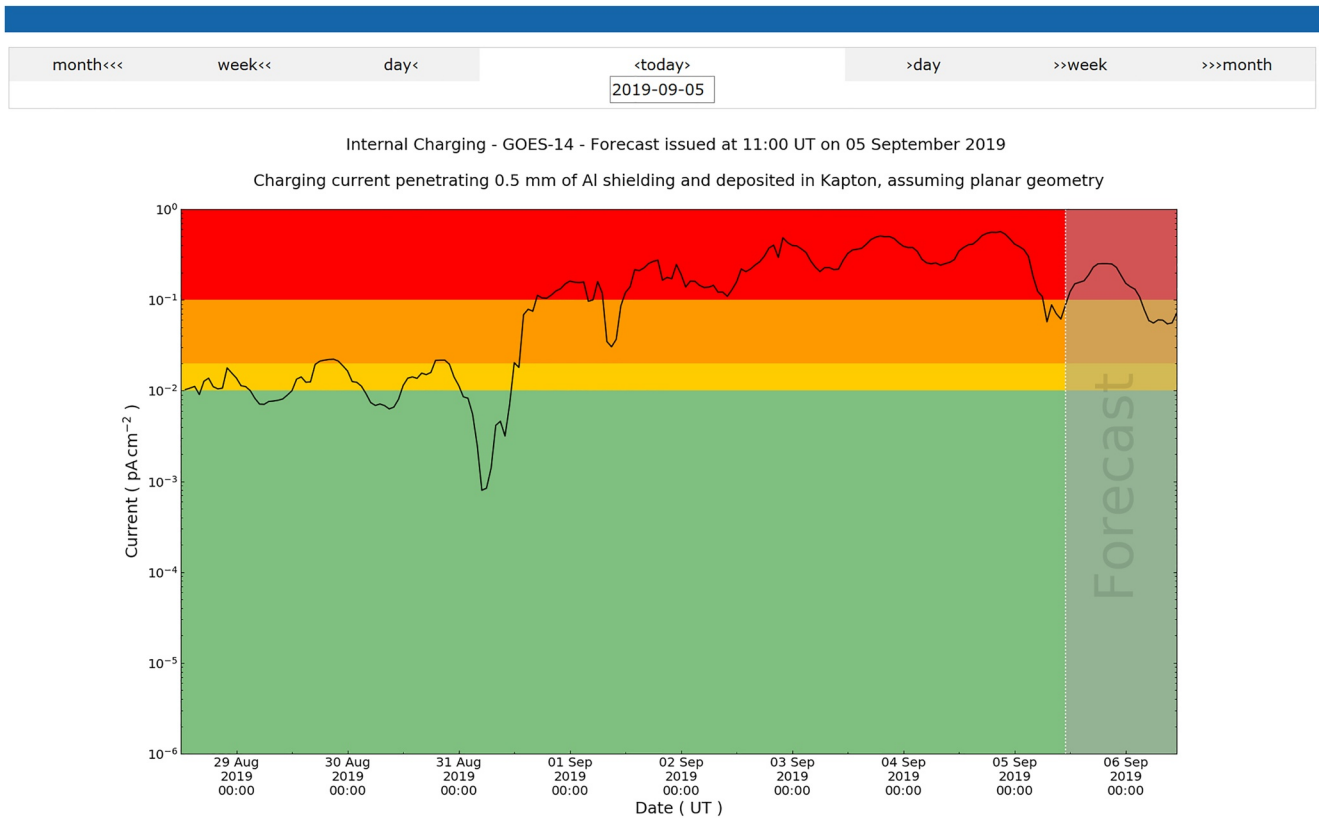
Figure 4. Internal charging current along the track of GOES 14. The current deposited in Kapton is calculated for 0.5 mm of Al shielding assuming planar geometry. The different colors correspond to different levels of risk of internal charging.

materials hotter than 25°C. Similarly the NASA Technical handbook states that if the incident flux corresponding to a current greater than 0.1 pA cm^{-2} then the components should be shielded so as to reduce the current to that level (NASA, 2011), and that if the incident flux corresponds to a current greater than 1 pA cm^{-2} then electrostatic discharge (ESD) problems may exist. To convert these levels into something more easily understandable we have introduced a risk indicator with four levels of risk according to the internal charging current. Red for >0.1 pA cm^{-2}, amber for >0.02 pA cm^{-2}, yellow for >0.01 pA cm^{-2} and green otherwise. Note that the highest level (red) is set according to the recommendation for a higher level of shielding on the basis that this provides operators more time to take action.

As medium Earth orbit is very important for satellite radio-navigation systems such as Galileo and GPS Figure 5 is included to show the charging currents along the track of GIOVE-A. In this case the electron spectrum is taken wholly from BAS-RBM as there are no data available. As GIOVE-A is in a circular orbit at approximately 23,300 km altitude with an inclination of 56° it goes through the radiation belts twice every orbit. The orbit period is approximately 14 hr 22 min. Hence the largest charging current occurs as the satellite crosses the magnetic equator at approximately $L* = 4.66$. Otherwise, the satellite samples much higher $L*$ at higher latitudes.

Figure 5 shows that after 1 September the charging current exceeds the highest risk level and is off scale. However, charging is limited to a relatively short period on each orbit. The cumulative charge is very important for assessing the risk of an ESD and this depends very much on the time constant of the dielectric material used in the components (Bodeau, 2010). It remains to be seen whether charge accumulation becomes a significant risk factor in future for Galileo and GPS type orbits. If it does this suggests that we should consider the time integrated or accumulated charge in relation to the breakdown potential of the dielectric material.
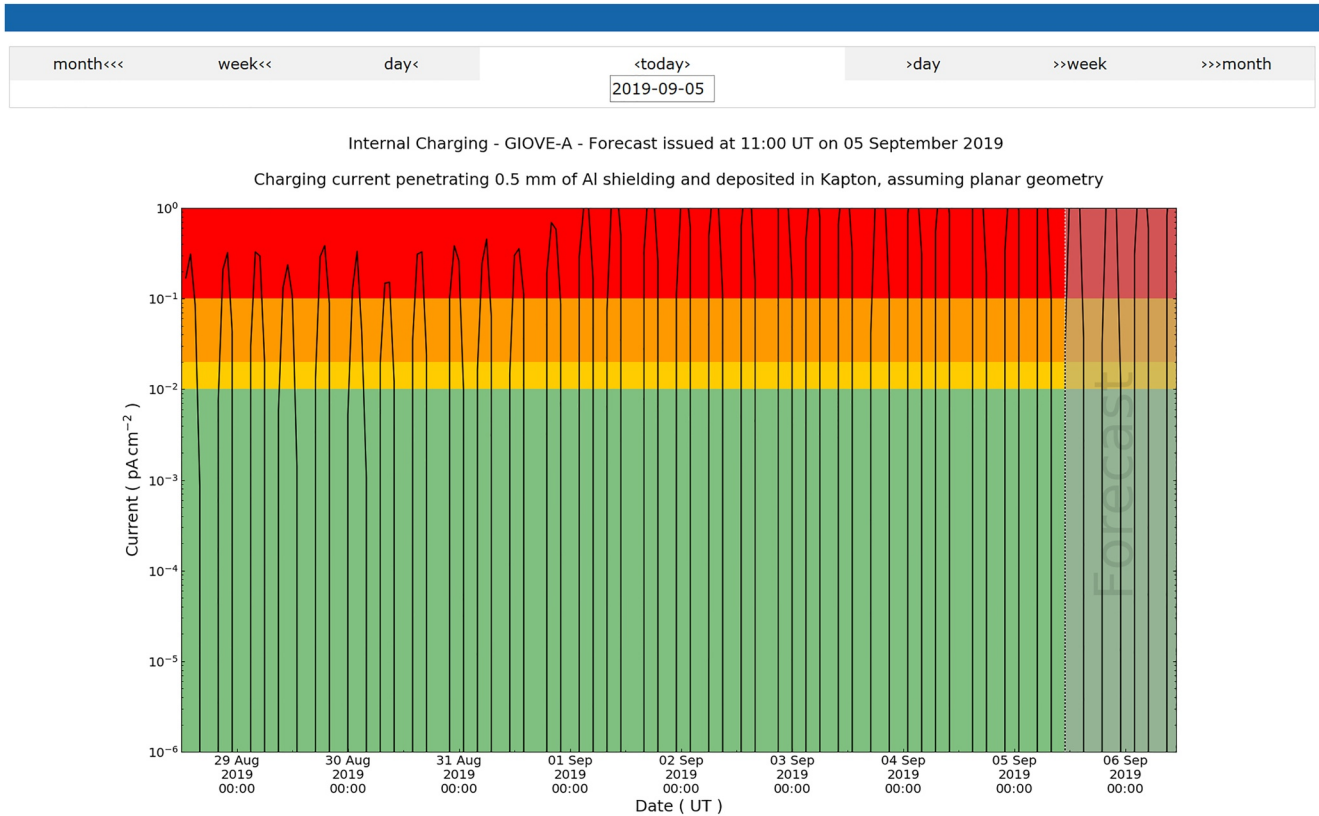
Internal Charging - GIOVE-A - Forecast issued at 11:00 UT on 05 September 2019

Charging current penetrating 0.5 mm of Al shielding and deposited in Kapton, assuming planar geometry

**Figure 5.** Same as Figure 4 but for GIOVE-A.

8. Dose Rate

The total ionizing dose (TID) is an important factor in the design of a satellite. As the dose increases it can result in the gradual degradation of components, performance and power consumption. It is one of the main design factors that can limit the lifetime of a satellite. The TID is the amount of radiation absorbed in matter due to all sources. In space this is mainly due to energetic electrons and protons arising from the radiation belts, high energy ions from a Solar Energetic Particle event and cosmic rays. As these particles are absorbed they emit Bremsstrahlung radiation, usually in the form of X rays, which is also absorbed later contributing to the total ionizing dose.

Although TID is very important for the lifetime of the satellite calculating it from the dose rate depends on when the satellite was launched and when it reached orbit. It also requires the continuous operation of SaRIF. Therefore, the dose rate is used as the risk indicator as it can be compared to the average expected dose rate. The risk levels for the dose rate have been set as red for $>5,000$ rads s^{-1}, amber for $>1,000$ rads s^{-1}, yellow for >100 rads s^{-1} and green otherwise.

The electron flux from BAS-RBM is used to calculate the electron and Bremsstrahlung dose rates along the satellite track using the SHIELDOSE-2Q code. In order to capture Solar Energetic Particle events, this is supplemented with proton dose rates using GOES near real time proton flux, with magnetic shielding applied for satellites in lower orbits such as MEO and the slot region, and the NASA AP-8/MAX model for the proton radiation belt. Unlike the electrons we cannot forecast the proton spectra and so the last proton spectra before the forecast is used for the entire forecast period. As ionizing dose is more appropriate for electronic components inside a shielded box rather than connectors outside and we have selected a total shielding of 2 mm of Al (0.5 mm for the satellite skin plus 1.5 mm) for the enclosure. Heavy ions are not included. Cosmic rays are not included, but the dose from cosmic rays is usually small compared to other sources.

In the SaRIF system the TID is also calculated from the dose rate since the start of operations. Therefore it is possible to test whether a satellite launched after the start of SaRIF (January 2019) is aging faster or slower than
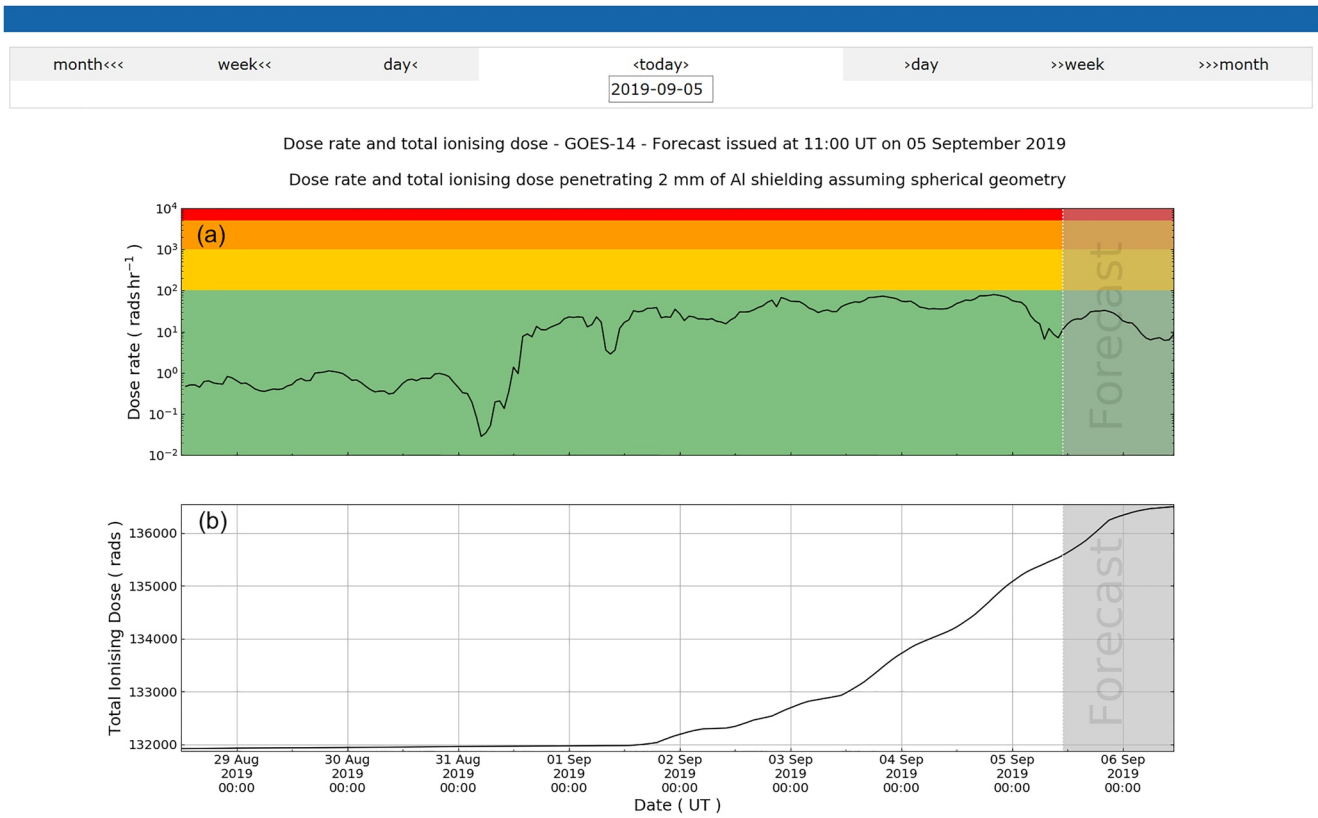
Figure 6. (a) Dose rate and (b) total ionizing dose along the track of GOES 14. The dose is calculated using the spectrum of electrons and ions for 2 mm of Al shielding and spherical geometry.

expected by inspecting the archive and taking the difference between time when first on orbit and the current value for the most representative orbit. During the first year of operation, which lasted until December 2019, there were only short breaks in the SaRIF system and so the TID was accumulated assuming zero dose rate while the system was down. The system stopped in January 2020 due to the change from GOES 14 and 15 to GOES 16 and 17 but is due to operate again later in 2021 whereupon the TID will be reset to zero.

Figure 6 shows an example of the dose rate and TID along the track of GOES 14. The dose rate increased significantly on 31 August corresponding to the increase in electron flux. As there was no SEP event at this time (Figure 2f) the increase was due to electrons. The TID (Figure 6b) increases steadily from half way through 1 September onwards.

Figure 7 shows an example of the differential (top) and integral (bottom) electron flux that was used in the forecasts. In this example, the flux was calculated by BAS-RBM on 5 September at 22:10 UTC corresponding to the forecast period for the GOES satellite. The proton spectrum measured by GOES 15 is shown in Figure 8 corresponding to 01:00 UTC on 5 September 2019. As well as forecasting, the spectra provide additional information to help resolve the cause of satellite anomalies and can be particularly important for other types of risks such as single event upsets. In particular, over the course of time they may help identify whether changes in the hardness of the spectra are important for satellite anomalies.

9. High Level Risk Summary

One of the key user requirements is to have a high-level summary of the risk. Figure 9 shows the SaRIF summary page for this event. The page is organized into a section on the radiation environment and a section on the risk indicators which can be accessed for each satellite indicated on the left. Two satellite orbits are available at geostationary orbit (GOES 14 and 15) to give an indication of the differences with longitude, one (GIOVE-A) to

BAS-RBM - Calculated GOES Electron Environment
05 September 2019 22:10 UTC
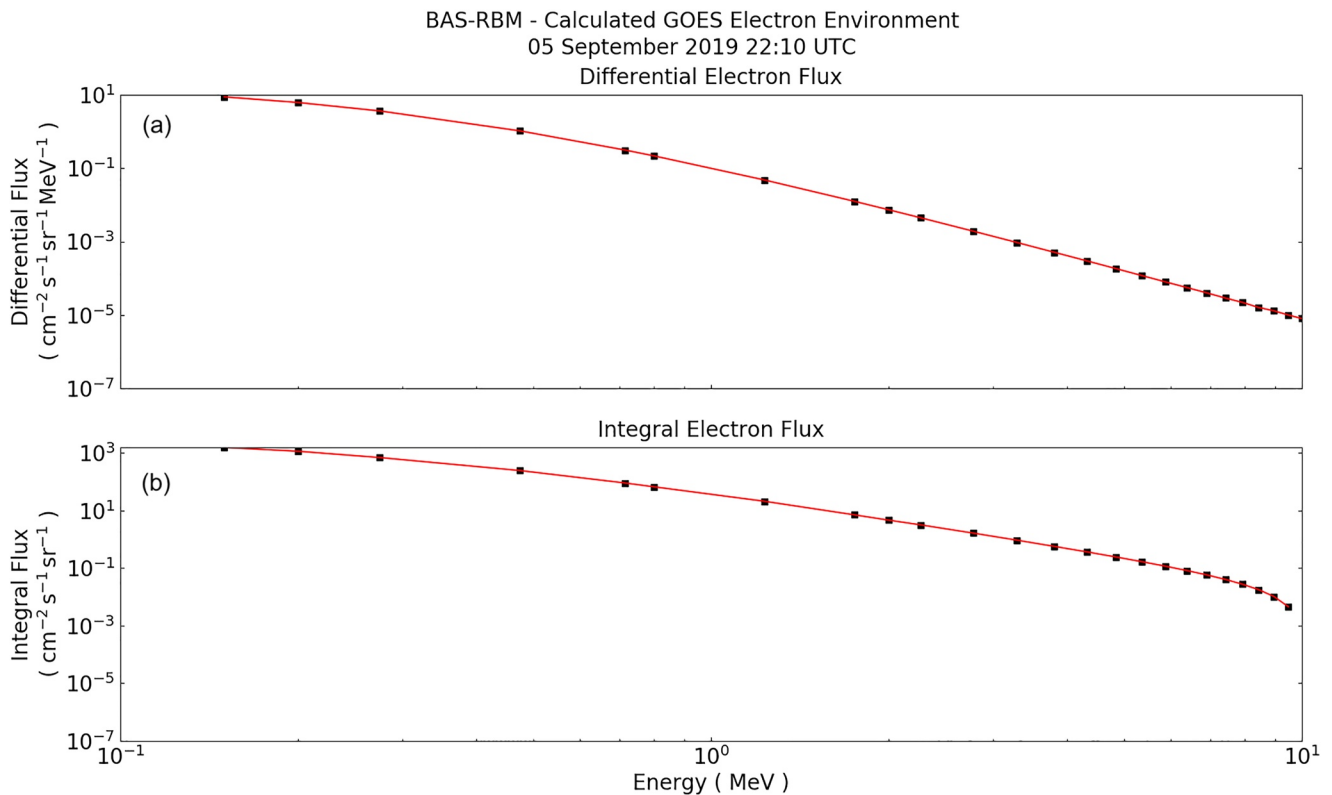
Figure 7. Electron flux (a) differential and (b) integral for geostationary orbit calculated by the BAS-RBM.

illustrate MEO and one to represent a circular orbit in the slot region for the O3b satellites at 8,000 km altitude. The risk indicators for internal charging and total ionizing dose are color coded according to the risk as described above.

Also included under the environment section is a link to outputs from the relativistic electron forecast model as run by the UKMO. Figure 10 shows an example which includes the average 1-, 2-, and 3-day forecast of the integral electron flux >2 MeV along with the measured values up to the present time. Also shown is the probability that a given threshold will be exceeded as forecasted by the Met Office Space Operations Center (MOSWOC), along with the MOSWOC summary. Thus, the combination of results from REFM, MOSWOC, and BAS-RBM provides complimentary information on longer term average forecasts for GEO together with more detailed information for different orbits and an assessment of risk.

A set of panels for post event reconstruction are also available from the front page, as shown in Figure 9. These contain the best reconstruction of the radiation environment using the BAS-RBM and are provided to help investigate the cause of satellite anomalies. They consist of the six panel plots similar to Figure 2 but without the forecast. They can differ slightly from the forecast runs since the final updated value of Kp is used to drive BAS-RBM instead of the forecast value and therefore the results should be more accurate. It is possible to step back through the plots a day, a week or a month at a time to help provide easy access for satellite operators and underwriters during their investigations. They provide an archive of different sources of data in one place and on the same timescale which may not be so easy to organize otherwise.

Since the SaRIF system went live in January 2019 GOES 14 and 15 have been taken out of service and replaced with GOES 16 and 17. Real-time data is only available from GOES 16 at present but historic data from GOES 17 is available. The SaRIF front page has therefore been adapted so that data from GOES 16 and 17 can be accessed and so that data from GOES 14 and 15 are still available via the post event reconstruction.
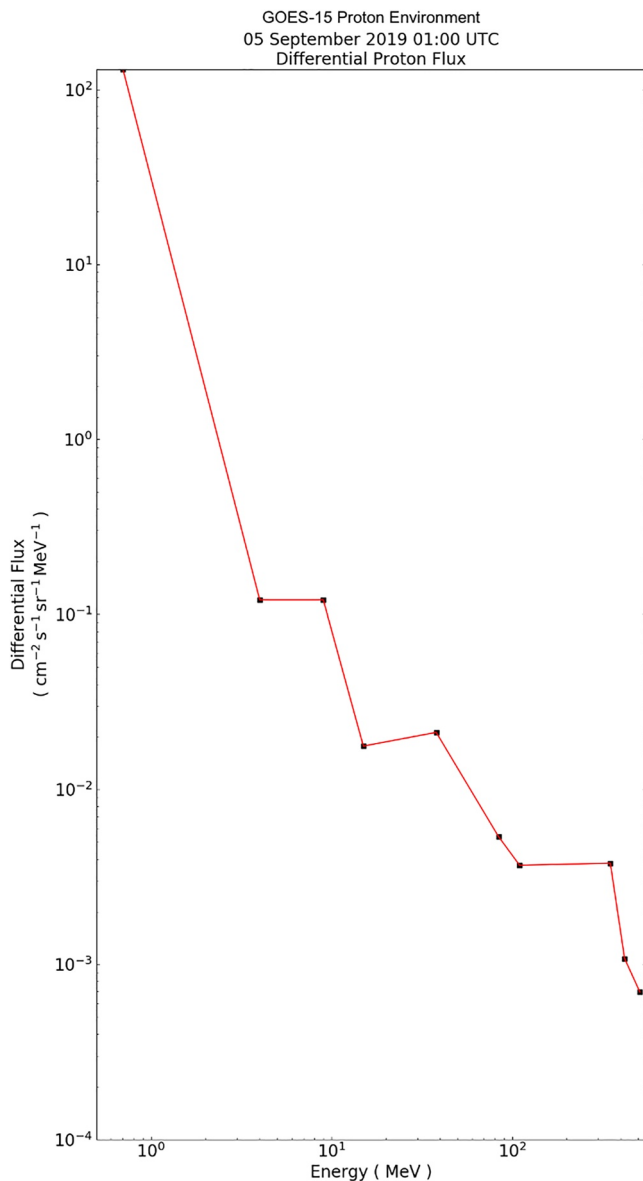
Figure 8. Differential proton flux measured by GOES 15.

10. Forecasting Skill

A detailed evaluation of the forecasting skill and accuracy of the reconstructions are given in the companion paper (Glauert et al., 2021). Only a short summary is given here. We should first recognize that since all the boundary conditions and diffusion coefficients depend on the forecast of Kp, an accurate forecast of Kp is essential. We also note that the Kp forecast provided by the Met Office Space Weather Operations Center (MOSWOC) is divided into intervals of 3 hr covering the next 24 hr (8 periods), and that the Kp forecast is produced by human forecasters originally intended for human consumption. The method is analogous to the early development of weather forecasting where humans used their skill and experience to add value. The forecasts are therefore considered to be an indicative representation of the next 24 hr. For example, if a Kp of 5 is possible in a 24 hr period then a Kp of 5 may be given in a particular 3 hr bin to indicate this possibility. However, the choice of a given bin depends on the skill of the forecaster as the observations preclude any high precision timing.

Here we take the forecast of Kp at face value and perform a point-by-point assessment on the 3 hourly Kp values, treating these deterministically. Many different metrics can be used to assess forecasts and here we highlight just one, the prediction efficiency (PE). The PE of these forecasts, which are compared here to a 6 months average between 1 March and 1 September 2019, is $PE = -1.14$. Since $PE > 0$ means we do better than a long-term average while $PE = 1$ means a perfect prediction, there is significant room for improvement. Work on improving the prediction of Kp will be reported elsewhere. Tests show that the BAS-RBM forecast of the >800 keV electron flux over a 1 hr period 24 hr ahead is $PE = 0.40$ and for >2 MeV is $PE = 0.62$ which are better than that for Kp. This indicates that changes in the radiation belt flux usually take longer than changes geomagnetic activity. A new system of improved initial conditions and boundary conditions has so far managed to achieve even higher prediction efficiencies with $PE = 0.59$ for >800 and $PE = 0.78$ for >2 MeV, over the same 6 month period as before, as described in the companion paper (Glauert et al., 2021). To set this in context the REFM forecast of the daily average flux >2 MeV over the next 24 hr is $PE = 0.7$ while other machine learning techniques achieve $PE = 0.82$ (Boynton et al., 2016). However, we emphasize there is no easy way to compare our results against these other forecast methods since they are predicting an average of the 24 hr flux over a complete orbit at GEO whereas we are predicting the flux over a 1 hr interval at a particular satellite location 24 hr ahead. It should also be noted that if there is a rapid variation in flux, such as a flux drop out, our forecasts will capture this variation more readily than a system that is only providing a 24 hr average since our forecasts are made hourly.

11. Discussion

The SaRIF system is a big step forward over that developed in SPACECAST in that it produces a forecast up to 24 hr as opposed to 3 hr. We have also spent considerable effort updating the boundary conditions which has improved the forecasting skill significantly. We have also revised some of the wave models and included EMIC waves so that the forecast and reconstruction of the radiation belts are more accurate, especially at higher energies. Even so there are still many areas where the forecasts can be improved.

One of the most easily implemented improvements would be a better forecast of Kp. At present the UKMO forecast of Kp is based on a number of factors including the current value, a time sequence taken from the previous
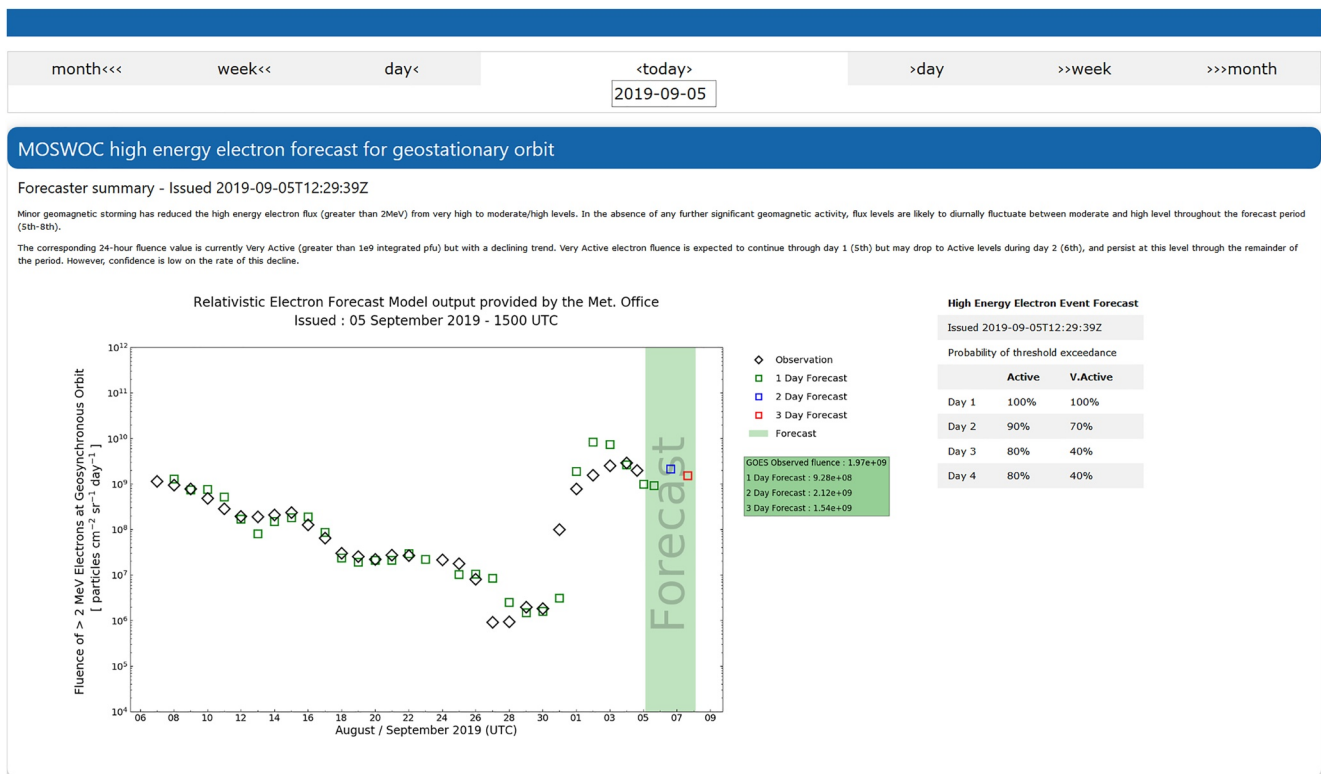
Satellite Risk Prediction and Radiation Forecasts

	Risk Indicators		Environment		
	Internal Charging	**Total Ionising Dose**	**BAS – Radiation Belt Model Forecast**	**Met. Office – Relativistic Electron Forecast Model**	**BAS – Post Event Reconstruction**
GOES-15	4	1	view plots	view plots at geostationary orbit	view plots
GOES-14	4	1	view plots		view plots
GIOVE-A	4	2	view plots		view plots
Slot Region 8000 km	1	1	view plots		view plots
Acknowledgements					

Time now : 5th September 2019 16:28 UT
Version 0.02.001

Figure 9. High level summary web page for the SaRIF system. The risk of internal charging and total ionizing dose are indicated by the numbers and color coding. The post event reconstruction panels hold an archive of data and model runs to help resolve the cause of satellite anomalies.

27-day solar rotation and forecaster experience. Thus, the Kp forecast can capture some of the effects resulting from features on the Sun which last longer than a solar rotation, such as coronal holes and fast solar wind streams. The method does not perform so well for coronal mass ejections and other processes which occur on shorter timescales and which can be highly disruptive. Thus, another system that translates solar observations into a

Figure 10. Display from the relativistic electron forecast model. The 1-, 2-, and 3-day average integral electron flux forecast for geostationary orbit are shown together with the actual measured flux. The MOSWOC probability of threshold exceedance is given in the inset panel along with MOSWOC forecaster summary text above.

forecast of Kp would be very helpful. Artificial intelligence (AI) or machine learning methods could play an important role here and work on this will be reported in future.

More generally, one might ask why use Kp at all, why not use AI methods to forecast the electron flux directly? Such methods have been developed using data from satellites at L1 to forecast the electron flux at GEO (Balikhin et al., 2016; Boynton et al., 2016). We are currently working on such methods and will report on this in future. However, these studies will always be limited to forecasting the flux at GEO and possibly LEO where there are considerable data available. If data from Galileo and GPS were made available this would also provide a considerable step forward. However, since these data only cover limited regions of space, a physics-based model will always be needed to give a complete picture. The ideal is probably a combination of AI methods to predict the flux at GEO, MEO, and LEO, and a physics-based model with data assimilation to give the full picture. Even then, such a system is very unlikely to predict the impact of a severe space weather event as there are not enough data on severe events to train AI systems. In this case research using physics-based models with different techniques (e.g., MHD models with particle tracing in realistic fields, Hudson et al. [1995]) which capture non-diffusive processes are essential to assess the likely impact.

It is sometimes said that Kp is not a good measure of geomagnetic activity and that using other indices such as the am index (Lockwood et al., 2019) or other coupling functions would be better. We have already established that scaling our diffusion rates by the AE index would give a better reconstruction (Glauert et al., 2018). However, unless a real-time forecast of these indices is provided we cannot use them. We could use the Burton equation to forecast Dst (Burton et al., 1975) but this is limited to a forecast of 45 min or so. Similarly, using measurements of the solar wind at L1 may provide a better forecasting skill but the time lag from L1 to Earth is still only about 30–45 min depending on solar wind speed. This could be extended if models such as WSA-ENLIL (Odstrcil, 2003) could provide accurate forecasts of the solar wind speed and IMF Bz further ahead in time. These forecasts are worth exploring and we will consider them in future. At present, Kp is the only index we know of that is forecast in real time up to 24 hr ahead, and available up to 27 days, and so our system is somewhat limited to the accuracy of Kp and the concept of persistence. In terms of the best reconstruction, we are likely to achieve a better reconstruction if we scale our diffusion coefficients and boundary conditions to other indices and use data assimilation methods. This will require data provision in a reasonable time, ideally within a few days. Data assimilation using a Kalman filter has been applied to other radiation belt models such as VERB (Kellerman et al., 2014; Shprits et al., 2013), DREAM (Reeves et al., 2012) and Salammbô (Bourdarie & Maget, 2012) and would help provide the best starting point from which to make the forecasts. We leave this for a future development.

One of the interesting results above is that the prediction efficiency for >2 MeV electron flux is higher than that for >800 keV. This is probably because convection and substorms drive changes in the lower energy flux but do not affect the higher energies as much due to the dominance of gradient and curvature drift at higher energies, and because it takes time to accelerate electrons to higher energies. By the same token it takes longer for loss by precipitation, except for very active times where we may reach the strong diffusion limit and changes in the magnetopause position and last closed drift shell can cause rapid outward diffusion.

There are a number of other areas where the forecasting model could be improved. The first is to reduce the uncertainty in the pitch angle and energy diffusion coefficients. For example, as the plasmapause is eroded to lower L^* the ratio of the electron plasma to gyrofrequency f_{pe}/f_{ce} just outside the plasmapause is likely to be lower than the average values used in our wave models. Chorus wave acceleration is very effective for low values of f_{pe}/f_{ce} (Allison & Shprits, 2020; Horne et al., 2003) and thus the MeV electron flux is likely to be underestimated. Electron acceleration by magnetosonic waves can also be very important (Horne et al., 2007) and should be included. Tests between the precipitation flux predicted by the model and that measured by the POES satellite show better agreement at 30 keV than at higher energies (Reidy et al., 2021). This also suggests that there is missing wave power in the model and more analysis is required.

The second key factor is to reduce the uncertainty in the radial diffusion coefficients. For example, there is evidence that the ULF waves that drive radial diffusion are much stronger during large magnetic storms and penetrate closer to the Earth as the plasmapause is eroded to lower L^* (Rae et al., 2019). Coupling of ULF waves driven by the solar wind on the outer magnetopause boundary to field line resonances at lower L^* may also drive stronger diffusion in certain regions. Under these conditions radial diffusion is likely to be far more effective than that in our model.

More generally, many research studies focus on particular events and adjust parameters and physical processes to reproduce those events. In doing so they identify some of the most important processes which leads to a big step forward in our understanding which is very valuable. Very often they result in an event specific set of diffusion coefficients or boundary conditions. The challenge is to translate these event specific conditions into something that can be used in a general model that can reproduce both the climatology of the radiation belts (Glauert et al., 2018) as well as severe events. For an operational system, the model has to do this using a limited set of observations provided by operational satellites in sparse locations. Scientific satellites which usually have more comprehensive measurements are usually limited to short mission lifetimes without continuous coverage between missions.

There is also the issue of approximating nonlinear wave-particle interactions by quasilinear theory which omits highly nonlinear effects such as particle trapping (Summers & Omura, 2007). These effects take place on a timescale of milliseconds and so to simulate the entire radiation belts over a period of 8 days or so some approximation has to be made to make the problem computationally tractable. So far, the quasilinear approximation seems to provide changes in the electron flux that agree well with the timescale for acceleration and loss on a global scale (Albert et al., 2009; Glauert et al., 2014b; Horne et al., 2005; Shprits et al., 2009; Varotsou et al., 2005) but there is still the concern as to whether the resulting diffusion rates are too large or too small or whether more nonlinear effects need to be incorporated.

Convective and non-diffusive processes are not included in our model. Our low energy boundary is set by a constant value of the first invariant μ where the lowest energy is about 150 keV. Convection is important below this energy but can sometimes affect higher energies (Allison et al., 2017). The omission of non-diffusive process is probably more important when changes in the solar wind operate on a timescale comparable to or faster than a drift period. One of the most important examples of this is the rapid compression of the magnetosphere by the solar wind in the March 1991 event (Blake et al., 1992). In this case, a new radiation belt was formed in 90 s by electrons which effectively "surfed in" on the induced electric field during just a fraction of their drift orbit. This event filled the slot region and would have affected the O3b satellite constellation if it had been operating at that time (Horne & Pitchford, 2015). Non-diffusive transport by ULF waves may also be important (Degeling et al., 2008). Again, other types of physics-based codes are more appropriate to address these effects which are more likely to occur in association with severe space weather events.

In the earlier SPACECAST system the flux at the low energy boundary and the outer boundary was derived from CRRES satellite data and was Kp dependent. Thus, the forecast of Kp was used to forecast the boundaries, select the diffusion coefficients and compute the flux throughout the radiation belts. This was later changed in the SPACESTORM project, and is also used in SaRIF, so that the flux at the outer boundary is derived from selecting a spectrum whose shape and magnitude depend on the >800 keV electron flux measured by GOES 15 (Glauert et al., 2018). The spectrum is assumed to persist for up to 24 hr in order to forecast compute the flux throughout the radiation belts (except for the special case where the last closed drift shell comes inside GEO). In principle one would like to simulate the whole outer belt for an inner region where $f = 0$ to an outer boundary where $f = 0$ but to do so requires the right balance between acceleration, transport and loss processes. This remains a considerable scientific challenge.

The charging current is a very useful risk indicator in that it can be compared to a design standard. However, that should not be the only consideration. The time constant of the dielectric material is also very important as for highly resistive dielectrics such as Kapton the charge may accumulate over very long timescales without significant leakage (Bodeau, 2010). Thus, over a period of weeks, possibly months, some dielectrics could charge to high levels so that even a relatively modest increase in flux could trigger an ESD. Ideally one would want to calculate the accumulated charge or electric field across the dielectric, but this would depend on the dielectric material and amount of radiation shielding which could vary considerably for one satellite to the next.

In the timeframe and resources available for the SaRIF development we were able to meet most but not all of the user requirements. In summary user requirements 1, 2, 4, 6, 8, and 9 have been met. Requirements 3, 5, and 10 are partially met. For requirement 3 on risk indicators, we provide risk indicators for internal charging and dose rate but we still need to develop additional risk indicators for surface charging, single event upsets and solar array degradation. The assessment of which risk is more important depends very much on the orbit type. For requirement 5 on orbit type, SaRIF covers GEO, MEO and the slot region but we still need to include HEO and LEO.

We should also distinguish between the traditional LEO below 1,000 km altitude, and high LEO above 1,000 km where the new satellite constellations are starting to operate. For LEO the effects of single event upsets are very important for high inclination satellites during solar energetic particle events and during passage through the south Atlantic anomaly region. We also need to consider how to address electric orbit raising to GEO where solar array degradation due to the proton belt (Lozinski et al., 2019) and electron radiation belt (Hands et al., 2018) become very important factors. For requirement 10 on data download we provide a searchable archive where plots can be captured for use locally but we still need to provide a comparison against previous severe events and a quantitative data download facility. We hope these requirements will be addressed in a future development.

12. Conclusions

We present a set of 10 user requirements that were obtained after extensive discussions with the satellite industry including satellite operators, designers, underwriters and space agency staff. Using these requirements as input, we have developed the SaRIF forecasting system which can be used to help maintain the safe and reliable operation of satellites on orbit and which provides an archive of radiation belt reconstructions that can be used to help identify the cause of a satellite anomaly. The key features of the SaRIF system are:

1. SaRIF addresses 10 users needs either fully (7) or partially (3) which were identified as a result of detailed discussions with satellite operators, designers, underwriters and Space Agency staff.
2. The SaRIF system provides forecast of high energy electron radiation throughout the outer radiation belt for the last 7 days and 1 day ahead. The forecasts are updated automatically every hour. The forecasts include data and model results for satellites in GEO, MEO and slot region orbits and allows the direct comparison between the model and the measured flux at several energies including the differential electron flux at 800 keV and 2 MeV, and the integral flux >800 keV and >2 MeV.
3. The radiation environment is used to calculate two risk indicators, the charging current behind a set level of radiation shielding and dose rate. These indicators are compared to design standards to assess the risk of damage. The TID since the start of the SaRIF system is also given and can be calculated for satellites launched at a later date by differencing the TID held in the archive.
4. The system provides a searchable archive of data and model reconstructions of the radiation environment to help identify the cause of a satellite anomaly.
5. The system provides a high-level summary of the radiation environment, risk indicators, and forecasts from the REFM in the form of color coded displays with the ability to drill down for more detailed information. The energy spectra for both electrons and protons are included.
6. The SaRIF system is freely available via the ESA space weather web portal.

The system has been updated to include data from GOES 16 and 17 which will be released later in 2021. We hope the system will be a valuable resource for both scientists and users in the space industry.

Data Availability Statement

The SaRIF forecasting system can be accessed from the ESA web portal (https://swe.ssa.esa.int/web/guest/sarif-federated). Forecasts of the Kp index are available on special request from the UK Met Office (https://doi.org/10.5285/bebfd99e-f2e3-46f0-9833-f59efb40be37). Other data include the Kp index from GFZ Helmholtz Centre, Potsdam (https://www.gfz-potsdam.de/en/kp-index/), AE and Dst index from the World Data Centre for Geomagnetism, Kyoto, Japan (http://wdc.kugi.kyoto-u.ac.jp/), GOES 14 and 15 electron and proton data from the NOAA data archive (https://satdat.ngdc.noaa.gov/sem/goes/data/avg), solar wind data from the DSCOVR Space Weather Data Portal (https://www.ngdc.noaa.gov/dscovr/portal/) and electron data from the RBSP satellites from (http://rbspgway.jhuapl.edu/). Data on charging currents from the SURF instrument on the GIOVE-A spacecraft are available on special request to the IGS Global Data Centre help desk (https://gssc.esa.int/contact/). Information on the Met Office provision of REFM can be accessed via SaRIF as given above. More information on REFM can be accessed on the Space Weather Prediction Center at (https://www.swpc.noaa.gov/products/relativistic-electron-forecast-model). The EMEC software is operated by DH Consultancy BVBA. Satellite position information is obtained from two line elements provided by Space Track (https://www.space-track.org/documentation) using NAIF/SPICE (https://naif.jpl.nasa.gov/naif/). The UNILIB software to calculate L^* is

available at (https://www.mag-unilib.eu/) and the magnetospheric shielding model at (http://www.sepem.eu/). The ESA open data interface (ODI) is at (https://essr.esa.int/project/odi-open-data-interface-server) and data retrieval OPeNDAP at (https://www.opendap.org). The results shown in this paper can be downloaded from the UK Polar Data Centre (https://data.bas.ac.uk/).

References

Albert, J. M., Meredith, N. P., & Horne, R. B. (2009). Three-dimensional diffusion simulation of outer radiation belt electrons during the 9 October 1990 magnetic storm. *Journal of Geophysical Research*, *114*(A9). https://doi.org/10.1029/2009JA014336

Allison, H. J., Horne, R. B., Glauert, S. A., & Zanna, G. D. (2017). The magnetic local time distribution of energetic electrons in the radiation belt region. *Journal of Geophysical Research: Space Physics*, *122*, 8108–8123. https://doi.org/10.1002/2017JA024084

Allison, H. J., & Shprits, Y. Y. (2020). Local heating of radiation belt electrons to ultra-relativistic energies. *Nature Communications*, *11*, 4533. https://doi.org/10.1038/s41467-020-18053-z

Baker, D. N., McPherron, R. L., Cayton, T. E., & Klebesadel, R. W. (1990). Linear prediction filter analysis of relativistic electron properties at 6.6 R_E. *Journal of Geophysical Research*, *95*(A9), 15133–15140. https://doi.org/10.1029/JA095iA09p15133

Balikhin, M. A., Rodriguez, J. V., Boynton, R. J., Walker, S. N., Aryan, H., Sibeck, D. G., & Billings, S. A. (2016). Comparative analysis of NOAA REFM and SNB^3 GEO tools for the forecast of the fluxes of high-energy electrons at GEO. *Space Weather*, *14*, 22–31. https://doi.org/10.1002/2015SW001303

Beutier, T., & Boscher, D. (1995). A three-dimensional analysis of the electron radiation belt by the Salammbô code. *Journal of Geophysical Research*, *100*, 14853–14861. https://doi.org/10.1029/94JA03066

Blake, J. B., Kolasinski, W. A., Fillius, R. W., & Mullen, E. G. (1992). Injection of electrons and protons with energies of tens of MeV into $L <$ 3 on 24 March 1991. *Geophysical Research Letters*, *19*, 821–824. https://doi.org/10.1029/92GL00624

Bodeau, M. (2010). High energy electron climatology that supports deep charging risk assessment in GEO. In *48th AIAA Aerospace Sciences meeting, 4–7 January 2010, Orlando, Florida* (pp. 1–13). https://doi.org/10.2514/6.2010-1608

Bourdarie, S. A., & Maget, V. F. (2012). Electron radiation belt data assimilation with an ensemble Kalman filter relying on the Salammbô code. *Annales Geophysicae*, *30*, 929–943. https://doi.org/10.5194/angeo-30-929-2012

Boynton, R. J., Balikhin, M. A., Sibeck, D. G., Walker, S. N., Billings, S. A., & Ganushkina, N. (2016). Electron flux models for different energies at geostationary orbit. *Space Weather*, *14*, 846–860. https://doi.org/10.1002/2016SW001506

Brautigam, D., & Albert, J. A. (2000). Radial diffusion analysis of outer radiation belt electrons during the October 9, 1990, magnetic storm. *Journal of Geophysical Research*, *105*, 291–309. https://doi.org/10.1029/1999JA900344

Burton, R. K., McPherron, R. L., & Russel, C. T. (1975). An empirical relationship between interplanetary conditions and *Dst*. *Journal of Geophysical Research*, *8*, 4204–4214. https://doi.org/10.1029/JA080i031p04204

Degeling, A. W., Ozeke, L. G., Rankin, R., Mann, I. R., & Kabin, K. (2008). Drift resonant generation of peaked relativistic electron distributions by Pc 5 ULF waves. *Journal of Geophysical Research*, *113*. https://doi.org/10.1029/2007JA012411

ECSS. (2020). *European Cooperation for Space Standardisation, ECSS-E-ST-10-04C Rev.1 – Space environment. Space Engineering: Spacecraft charging*. ESA Requirements and Standards Division, ESTEC. Retrieved from https://ecss.nl/standard/ecss-e-st-10-04c-rev-1-space-environment-15-june-2020/

Ganushkina, N. Y., Amariutei, O. A., Welling, D., & Heynderickx, D. (2015). Nowcast model for low-energy electrons in the inner magnetosphere. *Space Weather*, *13*, 16–34. https://doi.org/10.1002/2014SW001098

Glauert, S. A., & Horne, R. B. (2005). Calculation of pitch angle and energy diffusion coefficients with the PADIE code. *Journal of Geophysical Research: Space Physics*, *110*. https://doi.org/10.1029/2004JA010851

Glauert, S. A., Horne, R. B., & Kirsch, P. (2021). Evaluation of SaRIF high-energy electron reconstructions and forecasts. *Space Weather*, *19*(12), e2021SW002822.

Glauert, S. A., Horne, R. B., & Meredith, N. P. (2014a). Simulating the Earth's radiation belts: Internal acceleration and continuous losses to the magnetopause. *Journal of Geophysical Research: Space Physics*, *119*, 7444–7463. https://doi.org/10.1002/2014JA020092

Glauert, S. A., Horne, R. B., & Meredith, N. P. (2014b). Three dimensional electron radiation belt simulations using the BAS Radiation Belt Model with new diffusion models for chorus, plasmaspheric hiss and lightning-generated whistlers. *Journal of Geophysical Research: Space Physics*, *119*, 268–289. https://doi.org/10.1002/2013JA019281

Glauert, S. A., Horne, R. B., & Meredith, N. P. (2018). A 30-year simulation of the outer electron radiation belt. *Space Weather*, *16*, 1498–1522. https://doi.org/10.1029/2018SW001981

Hands, A. D. P., Ryden, K. A., Meredith, N. P., Glauert, S. A., & Horne, R. B. (2018). Radiation effects on satellites during extreme space weather events. *Space Weather*, *16*, 1216–1226. https://doi.org/10.1029/2018SW001913

Horne, R. B., Glauert, S. A., Meredith, N. P., Heynderickx, D., Boscher, D., Maget, V., & Pitchford, D. (2013). Space weather impacts on satellites and forecasting the Earth's electron radiation belts with SPACECAST. *Space Weather*, *11*, 169–186. https://doi.org/10.1002/swe.20023

Horne, R. B., Glauert, S. A., & Thorne, R. M. (2003). Resonant diffusion of radiation belt electrons by whistler-mode chorus. *Geophysical Research Letters*, *30*(9), 1493. https://doi.org/10.1029/2003GL016963

Horne, R. B., Kersten, T., Glauert, S. A., Meredith, N. P., Boscher, D., Sicard-Piet, A., et al. (2013). A new diffusion matrix for whistler mode chorus waves. *Journal of Geophysical Research: Space Physics*, *118*, 6302–6318. https://doi.org/10.1002/jgra.50594

Horne, R. B., Phillips, M. W., Glauert, S. A., Meredith, N. P., Hands, A. D. P., Ryden, K., & Li, W. (2018). Realistic worst case for a severe space weather event driven by a fast solar wind stream. *Space Weather*, *16*, 1202–1215. https://doi.org/10.1029/2018SW001948

Horne, R. B., & Pitchford, D. (2015). Space weather concerns for all-electric propulsion satellites. *Space Weather*, *13*, 430–433. https://doi.org/10.1002/2015SW001198

Horne, R. B., Thorne, R. M., Glauert, S. A., Albert, J. M., Meredith, N. P., & Anderson, R. R. (2005). Timescale for radiation belt electron acceleration by whistler mode chorus waves. *Journal of Geophysical Research*, *110*. https://doi.org/10.1029/2004JA010811

Horne, R. B., Thorne, R. M., Glauert, S. A., Meredith, N. P., Pokhotelov, D., & Santolık, O. (2007). Electron acceleration in the Van Allen radiation belts by fast magnetosonic waves. *Geophysical Research Letters*, *34*. https://doi.org/10.1029/2007GL030267

Hudson, M. K., Kotelnikov, A. D., Li, X., Roth, I., Temerin, M., Wygant, J., et al. (1995). Simulation of proton radiation belt formation during the March 24, 1991 SSC. *Geophysical Research Letters*, *22*, 291–294. https://doi.org/10.1029/95gl00009

Iucci, N., Levitin, A. E., Belov, A. V., Eroshenko, E. A., Ptitsyna, N. G., Villoresi, G., et al. (2005). Space weather conditions and spacecraft anomalies in different orbits. *Space Weather*, *3*. https://doi.org/10.1029/2003SW000056

Kellerman, A. C., Shprits, Y. Y., Kondrashov, D., Subbotin, D., Makarevich, R. A., Donovan, E., & Nagai, T. (2014). Three-dimensional data assimilation and reanalysis of radiation belt electrons: Observations of a four-zone structure using five spacecraft and the VERB code. *Journal of Geophysical Research: Space Physics*, *119*, 8764–8783. https://doi.org/10.1002/2014JA020171

Kersten, T., Horne, R. B., Glauert, S. A., Meredith, N. P., Fraser, B. J., & Grew, R. S. (2014). Electron losses from the radiation belts caused by EMIC waves. *Journal of Geophysical Research: Space Physics*, *119*, 8820–8837. https://doi.org/10.1002/2014JA020366

Lockwood, M., Bentley, S. N., Owens, M. J., Barnard, L. A., Scott, C. J., Watt, C. E., & Allanson, O. (2019). The development of a space climatology: 1. Solar wind magnetosphere coupling as a function of timescale and the effect of data gaps. *Space Weather*, *17*, 133–156. https://doi.org/10.1029/2018SW001856

Lozinski, A. R., Horne, R. B., Glauert, S. A., Zanna, G. D., Heynderickx, D., & Evans, H. D. R. (2019). Solar cell degradation due to proton belt enhancements during electric orbit raising to GEO. *Space Weather*, *17*, 1059–1072. https://doi.org/10.1029/2019SW002213

Meredith, N. P., Horne, R. B., & Anderson, R. R. (2001). Substorm dependence of chorus amplitudes: Implications for the acceleration of electrons to relativistic energies. *Journal of Geophysical Research*, *106*, 13165–13178. https://doi.org/10.1029/2000JA900156

NASA. (2011). *Mitigating in-space charging effects - a guideline, NASA Technical Handbook, NASA-HDBK-4002A*. National Aeronautics and Space Administration. NASA Technical Handbook.

Odstrcil, D. (2003). Modeling 3-D solar wind structure. *Advances in Space Research*, *32*, 497–506. https://doi.org/10.1016/S0273-1177(03)00332-6

Olson, W. P., & Pfitzer, K. (1977). Magnetospheric magnetic field modeling. *Annual Scientific Report*. AFOSAR Contract No. F44620-75-c-0033. https://doi.org/10.21236/ada037492

Oughton, E. J., Hapgood, M., Richardson, G. S., Beggan, C. D., Thomson, A. W. P., Gibbs, M., et al. (2019). A risk assessment framework for the socioeconomic impacts of electricity transmission infrastructure failure due to space weather: An application to the United Kingdom. *Risk Analysis*, *39*, 1022–1043. https://doi.org/10.1111/risa.13229

Rae, I. J., Murphy, K. R., Watt, C. E. J., Sandhu, J. K., Georgiou, M., Degeling, A. W., et al. (2019). How do ultra-low frequency waves access the inner magnetosphere during geomagnetic storms? *Geophysical Research Letters*, *46*, 10699–10709. https://doi.org/10.1029/2019GL082395

Reeves, G. D., Chen, Y., Cunningham, G. S., Friedel, R. W. H., Henderson, M. G., Jordanova, V. K., et al. (2012). Dynamic radiation environment assimilation model: DREAM. *Space Weather*, *10*(3). https://doi.org/10.1029/2011SW000729

Reeves, G. D., McAdams, K. L., Friedel, R. H. W., & O'Brien, T. P. (2003). Acceleration and loss of relativistic electrons during geomagnetic storms. *Geophysical Research Letters*, *30*(10). https://doi.org/10.1029/2002GL016513

Reeves, G. D., Spence, H. E., Henderson, M. G., Morley, S. K., Friedel, R. H. W., Funsten, H. O., et al. (2013). Electron acceleration in the heart of the Van Allen radiation belts. *Science Express*, *341*, 991–994. https://doi.org/10.1126/science.1237743

Reidy, J. A., Horne, R. B., Glauert, S. A., Clilverd, M. A., Meredith, N. P., Woodfield, E. E., et al. (2021). Comparing electron precipitation fluxes calculated from pitch angle diffusion coefficients to LEO satellite observations. *Journal of Geophysical Research*, *126*, e2020JA028410. https://doi.org/10.1029/2020JA028410

Rodgers, D. J., Ryden, K. A., Wrenn, G. L., Latham, P. M., Sorensen, J., & Levy, L. (2000). An engineering tool for the prediction of internal dielectric charging. In *Proceedings of the 6th Spacecraft Charging Conference, November 2–6, 1998* (pp. 125–130). AFRL Science Center, Hanscom AFB.

Roederer, J. G. (1967). On the adiabatic motion of energetic particles in a model magnetosphere. *Journal of Geophysical Research*, *72*, 981–992. https://doi.org/10.1029/JZ072i003p00981

Ryden, K. A., Morris, P. A., Ford, K. A., Hands, A. D. P., Dyer, C. S., Taylor, B., et al. (2008). Observations of internal charging currents in medium earth orbit. *IEEE Transactions on Plasma Science*, *36*(5), 2473–2481. https://doi.org/10.1109/TPS.2008.2001945

Seltzer, S. M. (1980). *SHIELDOSE: A computer code for space-shielding radiation dose calculations* (p. 1116). National Bureau of Standards. NBS Technical Note. https://doi.org/10.6028/nbs.tn.1116

Shprits, Y., Kellerman, A., Kondrashov, D., & Subbotin, D. (2013). Application of a new data operator-splitting data assimilation technique to the 3-D VERB diffusion code and CRRES measurements. *Geophysical Research Letters*, *40*, 4998–5002. https://doi.org/10.1002/grl.50969

Shprits, Y., Subbotin, D., & Ni, B. (2009). Evolution of electron fluxes in the outer radiation belt computed with the VERB code. *Journal of Geophysical Research*, *114*. https://doi.org/10.1029/2008JA013784

Shue, J. H., Song, P., Russel, C. T., Steinberg, J. T., Chaoa, J. K., Zastenker, G., et al. (1998). Magnetopause location under extreme solar wind conditions. *Journal of Geophysical Research*, *103*(17), 691–17700. https://doi.org/10.1029/98JA01103

Subbotin, D. A., & Shprits, Y. Y. (2009). Three-dimensional modeling of the radiation belts using the versatile electron radiation belt (VERB) code. *Space Weather*, *7*. https://doi.org/10.1029/2008SW000452

Summers, D., & Omura, Y. (2007). Ultra-relativistic acceleration of electrons in planetary magnetospheres. *Geophysical Research Letters*, *34*. https://doi.org/10.1029/2007GL032226

Tsurutani, B. T., & Gonzalez, W. D. (1987). The cause of high-intensity long-duration continuous AE activity (HILDCAAs): Interplanetary Alfven wave trains. *Planetary and Space Science*, *35*, 405–412. https://doi.org/10.1016/0032-0633(87)90097-3

Tu, W., Cunningham, G. S., Chen, Y., Henderson, M. G., Camporeale, E., & Reeves, G. D. (2013). Modeling radiation belt electron dynamics during GEM challenge intervals with the DREAM3D diffusion model. *Journal of Geophysical Research: Space Physics*, *118*, 6197–6211. https://doi.org/10.1002/jgra.50560

Tu, W., Cunningham, G. S., Chen, Y., Morley, S. K., Reeves, G. D., Blake, J. B., et al. (2014). Event specific chorus wave and electron seed population models in DREAM3D using the Van Allen Probes. *Geophysical Research Letters*, *41*, 1359–1366. https://doi.org/10.1002/2013GL058819

Tu, W., Xiang, Z., & Morley, S. K. (2019). Modeling the magnetopause shadowing loss during the June 2015 dropout event. *Geophysical Research Letters*, *46*, 9388–9396. https://doi.org/10.1029/2019gl084419

Varotsou, A., Boscher, D., Bourdarie, S., Horne, R. B., Glauert, S. A., & Meredith, N. P. (2005). Simulation of the outer radiation belt electrons near geosynchronous orbit including both radial diffusion and resonant interaction with whistler-mode chorus waves. *Geophysical Research Letters*, *32*. https://doi.org/10.1029/2005GL023282

Wrenn, G. L. (1995). Conclusive evidence for internal dielectric charging anomalies on geosynchronous communications spacecraft. *Journal of Spacecraft and Rockets*, *32*, 514–520. https://doi.org/10.2514/3.26645

Wrenn, G. L. (2009). Chronology of 'Killer' electrons: Solar cycles 22 and 23. *Journal of Atmospheric and Solar-Terrestrial Physics*, *71*, 1210–1218. https://doi.org/10.1016/j.jastp.2008.08.002